10. ELECTRICAL RESISTIVITY STRUCTURE OF THE YELLOWKNIFE RIVER FAULT ZONE AND SURROUNDING REGION

Alan G. Jones[1,2] and Xavier Garcia[1,2]

1. Geological Survey of Canada, 615 Booth Street, Ottawa, Ontario, Canada, K1A 0E9
2. Now at: Dublin Institute for Advanced Studies, 5 Merrion Square, Dublin 2, Ireland

INTRODUCTION

Electromagnetic data, using the natural-source magnetotelluric (MT) technique, were acquired in the southwestern part of the Archean Slave craton, northwestern Canada, as a contribution to two geoscientific programs to determine the crustal and lithospheric mantle electrical resistivity structure. As part of LITHOPROBE, Canada's national geoscience project (Clowes et al., 1999), during the summer of 1996 MT time series were recorded at twelve sites on the all-weather road along an approximately east-west profile, of direct-line length of 130 km, with the city of Yellowknife in its centre (Fig. 10-1, sites 003-014). Two additional Lithoprobe sites (Fig. 10-1, sites 032 and 033) were acquired in March, 1999 east of Yellowknife in lakes just north of the all-weather road (the Ingraham Trail). Subsequently, as part of EXTECH III activities, a profile of seven sites was recorded in March, 2000 across the surface trace of the Yellowknife River Fault Zone (Bleeker and Ketchum, 1998) some 10 km north of the first profile (Fig. 10-1, sites 101–107), plus an eighth site (site 045) along the LITHOPROBE profile.

The purpose of the LITHOPROBE surveys was to define the gross geological architecture of Canada, with its central aim of gaining a better understanding of how the North American continent evolved. Thus, the 1996 and 1999 LITHOPROBE sites recorded broadband MT (BBMT) and long period MT (LMT) data at frequencies suitable for regional-scale crustal probing with site spacing on the order of 15 km. In contrast, EXTECH is a program for detailed high resolution imaging of specific features related to mineral exploration, and accordingly high-frequency audio-MT (AMT) data were acquired at the EXTECH III sites, with approximately 2.5 km site spacing, for superior resolution of upper crustal structures, in particular of the Yellowknife River Fault Zone (YRFZ). The detailed locations of the sites in the vicinity of the YRFZ are shown in Figure 10-2. The primary objective of the EXTECH III MT study was to determine the electrical structure of the fault zone and its wall rocks, and relate it to crustal and lithospheric scale geometries that might have influenced the processes of mineralization at the nearby Con and Giant gold mines.

The process of faulting rocks invariably leads to changes in their physical properties and consequently in their electromagnetic characteristics. Strike-slip faults can often result in reduced electrical resistivity, and examples include the Paleozoic-Mesozoic (Neoproterozoic?) Great Glen Fault in Scotland (Kirkwood et al., 1981), the Eocene-aged Fraser Fault in southwestern British Columbia (Jones et al., 1992), and the uppermost crustal sections of the modern San Andreas Fault in California (Unsworth et al., 1997, 1999; Park and Roberts, 2003). The causes for conductivity enhancement in strike-slip faults range from fluids in gauge zones to sulphides, iron oxides, and graphite deposited by fluid precipitation processes. In contrast, other major strike-slip faults show resistive crust below them, including the Paleoproterozoic Great Slave Lake Shear Zone (Wu et al., 2002), the Eocene-aged Tintina Fault in the Yukon Territory and northern British Columbia (Ledo et al., 2002), and the middle crustal section of the San Andreas Fault at Carrizo Plain (Mackie et al., 1997). Clearly, processes during and subsequent to strike-slip faulting are not uniform and do not lead to similar conductivity structures within the fault zone.

This paper will examine the LITHOPROBE and EXTECH III MT data and present and interpretation of the electromagnetic characteristics of the rocks involved in the Yellowknife River Fault Zone.

GEOLOGICAL SETTING

The study region lies in the southwestern part of the Archean Slave craton of northern Canada. The Slave craton is approximately 700 km (north-south) by 500 km (east-west) in exposed extent and hosts the Acasta gneisses, currently the oldest dated rocks on Earth (4.027 Ga, Stern and Bleeker, 1998). It is divided into a west-central basement complex, named the Central Slave Basement Complex by Bleeker et al. (1999a,b), and an eastern domain, named the Hackett River Terrane by Kusky (1989) and the eastern Slave Province by Bleeker et al. (1999a,b). The boundary between the two is thought to be a ~2.7 Ga suture (e.g. Kusky, 1989; Davis and Hegner, 1992; Bleeker et al., 1999a,b), and its location is reasonably well approximated by the Pb isotope line of Thorpe et al. (1992), and the Nd isotope line of Davis and Hegner (1992), recently extended to the southeast by MacLachlan et al. (2001). The pertinent aspects of the geology are described below.

The premise for this study stems from questions regarding the relationship between the two major lithological packages, the Kam Group and the Banting Group rocks, that comprise the Yellowknife greenstone belt. The interpretation of the stratigraphy of the belt has evolved considerably (Helmstaedt, 2006) but the most recent interpretation views the volcanic belt as representing two cycles of volcanism,

Jones, A.G. and Garcia, X.
2006: Electrical resistivity structure of the Yellowknife River Fault zone and surrounding region; Chapter 10 *in* Gold in the Yellowknife Greenstone Belt, Northwest Territories: Results of the EXTECH III Multidisciplinary Research Project, (ed.) C.D. Anglin, H. Falck, D.F. Wright, and E.J. Ambrose; Geological Association of Canada, Mineral Deposits Division, Special Publication No. 3, p. 126-141.

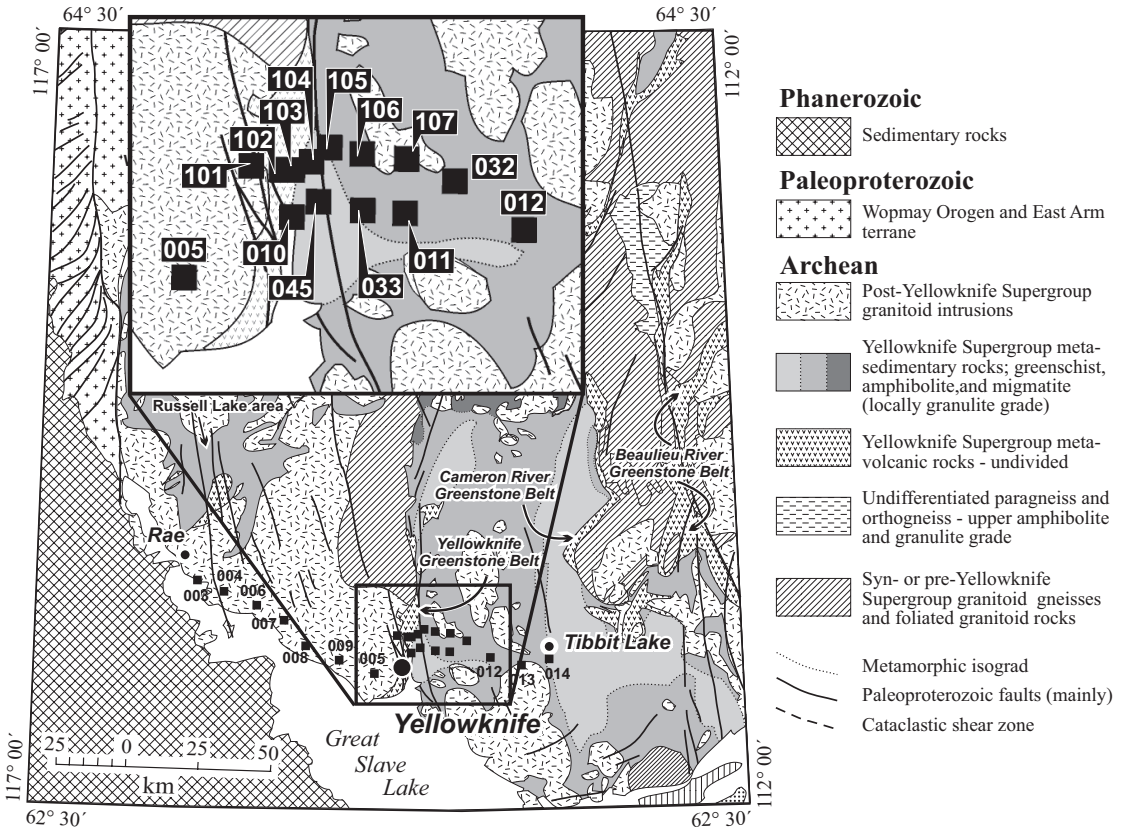

Figure 10-1. Location of the magnetotelluric sites on bedrock geology based on the map of J.B. Henderson (1998). The inset shows the sites around the Yellowknife River Fault Zone.

the tholeiitic Kam Group overlain by the calcalkaline Banting Group. The Banting Group has been divided into the Ingraham and Prosperous formations separated by the Walsh Formation, both of which are conformably overlain by the turbiditic sediments of the Burwash Formation that fill the Yellowknife Basin east of the volcanic belt. Helmstaedt and Padgham (1986) interpreted the sequence to be homoclinal and east facing with two cycles of felsic volcanism separated by the deposition of the Walsh Formation. The contact relations between the Kam Group and the Banting Group were defined differently in different parts of the belt. In the northern portions of the belt, the contact relationship was unconformable, but in the southern reaches of the belt, the relationship was more gradational and conformable (Helmstaedt and Padgham, 1986).

Isotopic analyses by Cousens et al. (2002) demonstrated that mafic rocks of the Banting and Kam groups are similar in composition, but felsic rocks are distinctive. The isotope systematics and incompatible element patterns in Kam Group rocks are consistent with combined fractional crystallization and crustal contamination of upper mantle-derived primitive magmas to form the more evolved magmas (Cousens, 2000). Felsic rocks in the Banting Group do not consistently have more negative ε_{Nd} than Banting mafic rocks, but instead are generally positive, suggesting that Banting felsic rocks could not have evolved by the same magma sources that produced the Kam Group. Using this distinction, Falck et al. (1999) and Cousens et al., (2006) were able to demonstrate that the rocks previously assigned to the Banting Group in the southern portions of the belt actually belonged to the Kam Group, and only rocks intersected by drillholes under the centre of Yellowknife Bay had Banting Group affinities.

This interpretation demonstrates that the contact between the Kam and Banting groups is defined by the Yellowknife River Fault Zone (Bleeker and Ketchum, 1998) along it entire length, commonly obscured by an infilling of younger conglomerates belonging to the Jackson Lake Formation (Falck et al., 1991), and this raises questions on the true relationship between the major lithological packages. The presence of this Archean structure has been previously postulated (e.g. Pettijohn, 1970; Helmstaedt and Padgham, 1986; Bailey, 1987; Mueller and Donaldson, 1994; Bleeker and Ketchum, 1998) and further analyzed by Martel et al. (2006). The fault zone has been traced from Shot Lake to Quyta Lake, extending for over 40 km, but can be extended further north and connecting with the Ormsby Break (Stubley et al., 1997) and south beneath Yellowknife Bay (H. Falck, pers. comm., 2001). Where the fault is exposed south of Greyling Lake, the zone is spatially associated with the Jackson Lake Formation-Banting Group contact and strikes north-northeast. North of Greyling Lake, the Jackson Lake Formation has not been preserved and the fault zone defines the Kam-Banting contact.

In addition to the Archean fault zones, the Yellowknife greenstone belt is transected by a complex system of brittle faults that transect all of the lithologies, including the Proterozoic age mafic dykes. These north- to northwest-trending, subvertical faults are sharp, narrow fractures with minor wall-rock brecciation and occasionally a clay-like gouge fill (Henderson and Brown, 1966). The faults offset and overprint the Archean structures, completing the interpretation of the older deformation zones. However, the movement of the younger faults, which include the West Bay, Hay-Duck, and Akaitcho faults, is mainly transcurrent and sinistral.

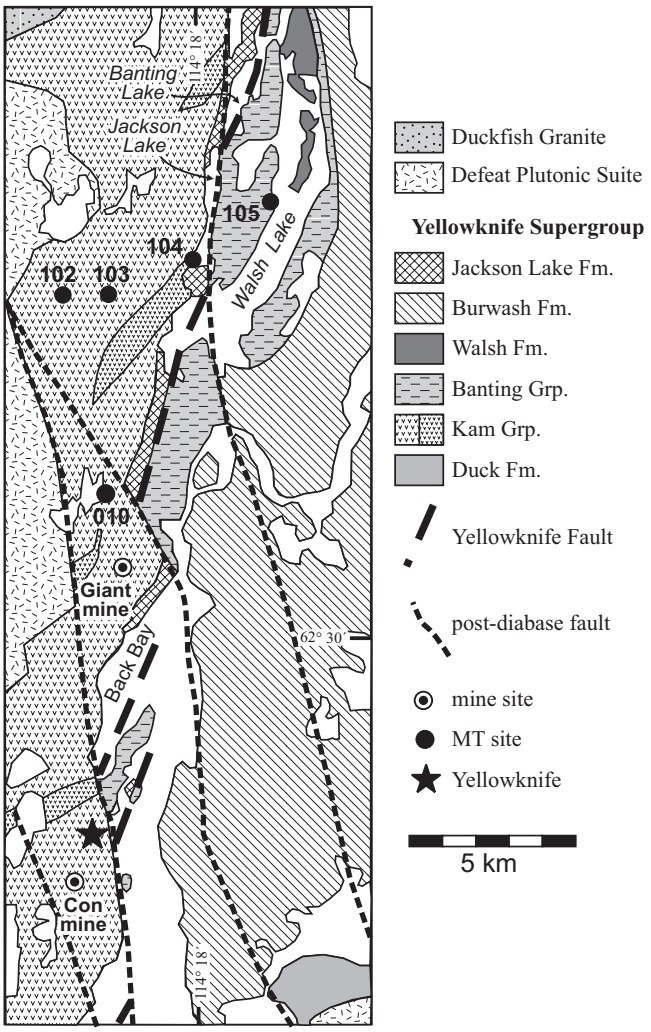

Figure 10-2. Detailed geology and MT site locations in the vicinity of the Yellowknife Fault (redrawn from Martel et al., 2002; Fm. = Formation, Grp. = Group).

MAGNETOTELLURIC METHOD AND DATA ACQUIRED

The Magnetotelluric Method

The magnetotelluric method is a natural-source electromagnetic surveying technique that was proposed independently on theoretical grounds by Tikhonov (1950, reprinted in Vozoff, 1986) in Russia and Cagniard (1953, reprinted in Vozoff, 1986) in France in the early 1950s. Cagniard's paper, published in English in the widely read Society of Exploration Geophysicists' journal Geophysics, received some attention, and attempts were made through the 1950s to use the proposed technique. The results were discouraging because of their nonrepeatability and large scatter of MT response estimates yielding poor resolution of structures. However, significant developments since that time in all aspects of the method, (those up to the early 1980s are recorded in the reprints volume of Vozoff, 1986) have resulted in the method being now repeatable, reliable, and able to give high resolution models of the subsurface that can be correlated with other geophysical results (principally from seismology, both passive and active), geology, and geochemistry. General discussions of the MT method and its application can be found in Jones (1992, 1993, 1998, 1999).

The sources of natural electromagnetic radiation are distant lightning storms at high frequencies (>8 Hz), and the interaction of ejected solar plasma with the Earth's magnetosphere at low frequencies (<10 Hz). The energy from either source is trapped in the waveguide between the Earth's surface and the ionosphere, at a height of ~100 km, and can travel around the Earth many times before being attenuated to below sensor noise levels. The magnetic fields from these sources penetrate into the Earth, and, by Faraday's Law of Induction, induce electrical fields. The strength of the electric currents associated with those fields is directly proportional to the electrical conductivity of the rocks by Ohm's Law (see below). So, essentially, in the magnetotelluric method one observes on the surface of the Earth both the inducing field and the induced field and thereby can deduce information about the conductivity structure. The complex ratio between the electric and magnetic fields is called the *impedance*, and the impedance is scaled in terms of its squared-magnitude and its phase to give the MT *apparent resistivity* and *phase* data from:

$$\rho_{xy}(f) = \frac{1}{2\pi f \mu}\left|Z_{xy}\right|^2$$

and

$$\phi_{xy}(f) = \arctan(\mathrm{imag}(Z_{xy}) / \mathrm{real}(Z_{xy}))$$

and the MT apparent resistivity can be thought of as similar to the apparent resistivity in DC resistivity methods. For a uniform half-space, the MT apparent resistivity gives the true resistivity of the half space.

In addition to the ratio of the magnitudes, MT has the advantage of measuring the phase difference of the electric field variations to the magnetic field ones. The phase difference is 45º for a uniform Earth, and rises above 45º when the underlying layer is less resistive than the layer above, and below 45º when the underlying layer is more resistive than the one above. For one-dimensional and two-dimensional Earths, phase is bounded between 0º for a perfect insulator at depth, and 90º for a perfect conductor at depth.

In essence, the method relies upon two well-known physical phenomena. One comes from Michael Faraday's Law of Induction and is the *skin depth effect* by which EM fields are attenuated in a medium of finite electrical conductivity. The skin depth δ (in kilometres) in a medium of resistivity ρ (in Ω.m) at a period of f (in Hertz) is given by:

$$\delta(f) = 503\sqrt{\rho / f}$$

from which one can appreciate that penetration increases with decreasing frequency. For a medium of constant resistivity, ρ, then as the frequency decreases the penetration depth, δ, increases. In a one-dimensional (1-D) Earth where resistivity varies with depth alone, then for a simple two-layered Earth the high-frequency apparent resistivities give the upper layer resistivity, and as one determines the results for the progressively lower frequency, a series of resistivity val-

ues is calculated that asymptotically approach the true value of the lower layer resistivity.

The second well-known physical phenomenon is the law of Georg Simon Ohm, or Ohm's Law, which is known as $V = I \bullet R$. By this law, the voltage in an electrical circuit is given by the electrical current times the resistance of the circuit. In a single medium through which electrical energies are transferred, the law can be rephrased in terms of vector current density J, vector electric field E, and (for simplicity) isotropic uniform electrical resistivity r, and is $\underline{E} = \underline{J} \bullet \rho$, or, in terms of current density, $\underline{J} = \underline{E} / \rho$. However, as rocks or other media are rarely uniform, the response of the current to media of differing resistivities must be determined. Continuity conditions at the interface between two media of differing resistivity ρ_1 and ρ_2 require that the current density (the number of charges, electrons or ions, flowing through a one-square-metre loop in one second) normal to the interface be continuous, thus $J_{n1} = J_{n2}$. This requires that $E_{n1} / \rho_1 = E_{n2} / \rho_2$ by Ohm's Law, and as the resistivities are discontinuous, then so must the electric field normal to the interface be discontinuous. This is accomplished by the impinging of charges on the interface, and is well described in Price's (1973) excellent review where he calls these charges "*the villains of the piece*". These electric charges on conductivity discontinuities are sensed by the MT method due to the discontinuity in the apparent resistivities on either side of the interface, which gives it high sensitivity to the location of sub-vertical faults. — an advantage that MT has over seismic reflection methods.

Application of the MT method involves measuring the horizontal components of the time-varying electric and magnetic fields. These time series are then Fourier transformed into the frequency domain, and, using robust statistical methods (see, e.g., Jones et al., 1989), estimates are made of the impedance tensor elements at each frequency. These estimates are analyzed for distortion and for regional strike information, and an appropriate two-dimensional interpretation co-ordinate system is determined. The regional data, corrected for distortion, are modelled using modern two-dimensional (2-D) inversion algorithms, and the models are compared to other information, such as seismology, geology, petrology, and geochemistry.

In addition, usually the time-variations of the vertical magnetic-field component (Hz) are also recorded, and the relationship between that component and the horizontal magnetic components is determined from:

$$Hz(f) = Tzx(f) \bullet Hx(f) + Tzy(f) \bullet Hy(f)$$

and the two complex transfer functions Tzx and Tzy are termed the Geomagnetic Transfer Functions (GTFs). For a uniform source field, the GTFs are zero over a 1-D pancake-like layered Earth. The GTFs are often represented in terms of *induction vectors*, and the real vector, when reversed, usually points towards regions of enhanced conductivity (Jones, 1986). This is highly dependent on the assumption that the source of the electrical impulses is uniformly distributed and of constant strength, and fortunately at most locations the Earth is not nearly as uniform as the sources. At high latitudes, however, care must be taken to avoid non-uniform source fields causing problems with the data, and Jones and Spratt (2002) developed a simple method for deriving the MT and GTF responses as uncontaminated as possible.

For induction in a two-dimensional (2-D) Earth, the governing Maxwell equations can be written in terms of two sets of equations. One set of equations describes induction of currents that flow *along*, or parallel to, structures, and is termed the *Transverse Electric*, or TE, mode of induction. The other set describes induced currents that flow across, or perpendicular to, structures, and is termed the *Transverse Magnetic*, or TM, mode of induction. These terms come from electrical engineering, and have become somewhat reluctantly accepted by the global EM induction community. Other terms used for these two modes that one sees in the literature are *E-polarization* or *E-parallel* for TE, and *B-* or *H-polarization* or *E-perpendicular* for TM, respectively.

In a fully three-dimensional (3-D) Earth then, there is no separation possible into different modes of induction, and a fully 3-D model needs to be developed to explain the data (e.g., Jones et al., 2003).

Data Acquired

The MT data that were acquired along the regional and high-resolution profiles comprised three types and used four different MT recording systems. High-frequency audio-magnetotelluric (AMT) data acquire MT fields typically in the frequency range of 10,000 to 10 Hz, and thereby "see" the top part of the crust to about 5 to 10 km. Broadband MT (BBMT) data typically acquires frequencies in the band 1,000 to 0.001 Hz, and usually images the entire crust, but with less resolution of the near-surface features than AMT data. Long period MT (LMT) data are at frequencies of 0.1 to 0.0001 Hz, and probe the deepest crust and lithospheric mantle, usually to the lithosphere-asthenosphere boundary.

On the LITHOPROBE regional profile AMT, BBMT, and LMT data were acquired at most sites, but on the high-resolution profile only AMT and BBMT data were acquired. The AMT and BBMT data were acquired using Phoenix V5 (1996 survey) and V5-2000 (1999 survey) systems, and Metronix GMS-06 systems (2000 survey), whereas the LMT data (1996 survey only) were acquired using the GSC-designed LiMS (long period magnetotelluric system) systems (Andersen et al., 1988).

Due to the instrumentation available at the time, the data acquired on lakes (032, 033, 045) did not record the vertical magnetic field component (Hz), and therefore there are no geomagnetic transfer functions (GTFs) for those sites. Also, the sites on the high-resolution profile, sites 101 to 107, did not record Hz data. Along the EXTECH III high-resolution profile, the Yellowknife Fault, as mapped on the surface, passes between sites 104 and 105 close to site 104 (Fig. 10-2). At this location the Archean Yellowknife Fault is offset by the Proterozoic merged Hay-Duck-Yellowknife River Fault.

Data Processing

The data were processed to frequency-dependent MT impedance tensor estimates and geomagnetic transfer function estimates (where Hz was recorded) using robust processing codes (e.g., Jones et al., 1989) with remote-reference noise

reduction (Gamble et al., 1979). The BBMT data were processed by the commercial contractors, Phoenix and Geosystem, for the V5 and GMS data respectively. Phoenix uses a cascade decimation code (Wright and Bostick, 1980), with the addition, implemented by Jones, of the Jones-Jödicke robust estimation scheme (Jones and Jödicke, 1984; method 6 in Jones et al., 1989). Geosystem uses Larsen's approach (Larsen, 1989; Larsen et al., 1996).

The LMT data were processed by the authors using the multi-remote reference robust code of Jones, referred to above. Contamination from possible source field effects on the LMT response estimates was reduced using the approach of Jones and Spratt (2002). An example of the source-field contamination problems is shown in Jones and Spratt for site 007 (named 107 in Jones and Spratt, 2002). The mantle lithosphere would be thought to be too conductive without applying this procedure.

ANALYSES FOR REGIONAL GEOELECTRIC STRIKE

Prior to modelling the MT response estimates, it is important to determine the regional dimensionality of the electrical structures, i.e., whether they are 1-D, 2-D or 3-D. If the data are deemed to be interpretable in terms of two-dimensional (2-D) structures, the characteristic geoelectric strike direction of the subsurface structures, as defined by the MT data, must also be derived. This step is crucial, as the surface geological strike may not be appropriate for the whole crust, as shown in Marquis et al. (1995) and Wu et al. (2002). In the former, the general N25ºW strike of the morphogeological belts in the southern part of the Canadian Cordillera was shown to be appropriate only for the top 7 to 10 km of the crust, below which the geoelectric strike becomes N20ºE, consistent with North American affinity rocks (Marquis et al., 1995). In Wu et al. (2002), the geoelectric strike for stations around the Great Slave Lake shear zone was shown to be ~N30ºE in the crust, and ~N60ºE in the mantle.

Before the mid-1980s strike was determined using methods largely based on the amplitudes of the impedance tensor. However, problems with amplitude distortions of primarily the electric field, caused by local, near-surface inhomogeneities, resulted in inconsistent strike determinations on a site-by-site basis for many surveys, thus leading to inappropriate strike directions being adopted.

Once the nature of the distortions was better understood, methods for strike determination were developed that used the phase information within the MT impedance tensor, rather than the strike information. Bahr (1984) was the first to recognize the symmetry in phase required by a 2-D Earth subsurface, based on the 2-D electric field distortion extension of Richards et al. (1982) of the 1-D approach of Larsen (1977). A number of approaches have been proposed for analysis of the MT impedance tensor to derive the strike direction, regional impedances, and distortion parameters (Bahr 1988, 1991; Bailey and Groom, 1987; Zhang et al., 1987; Groom and Bailey, 1989, 1991; Chakridi et al., 1992; Smith, 1995, 1997). Of these, the approach of Groom and Bailey (Bailey and Groom, 1987; Groom and Bailey, 1989, 1991), offers advantages over the others – it uses a physical model for distortion in terms of determinable and indeterminable parameters, derives the best-fitting model of distortion fitting the data, and provides a firm statistical basis for accepting whether the distortion model is appropriate. Groom et al. (1993) and Jones and Dumas (1993) describe a step-by-step methodology for applying the Groom and Bailey approach. Recently, McNeice and Jones (2001) presented a multi-site, multi-frequency approach for applying Groom and Bailey distortion decomposition to a set of sites, and we apply McNeice and Jones distortion decomposition herein. The determinable distortion parameters in Groom and Bailey analysis are termed twist and shear. These two describe the distortion of the electric field through rotation and anisotropic amplitude effects and are estimated from the effects on the phase data. Shear is limited to a range of ±45°, at which the impedance tensor becomes singular. Twist varies between of ±60°. The indeterminable ones relate to pure amplitude scaling, and only affect the apparent resistivity data not the phase data. These are also called static shifts (Jones, 1988), as the effect is to shift the apparent resistivity curves vertically on a logarithmic ordinate scale by a static amount, which does not change the shape of the curves. Static shifts are one of the banes of the MT method, and a number of solutions have been proposed for addressing the problem.

McNeice and Jones distortion decomposition has been applied to the data from both the regional and high-resolution profiles. The decompositions have been determined in both multifrequency and multisite modes. The geoelectric strike directions in decade-wide frequency bins, on an individual site basis, are shown in Figure 10-3. The strike directions represent the best-fitting strike direction at each site over all data within the frequency bin indicated. The length of the arrow denotes the averaged phase difference over the frequency bin between the phases in the strike direction and the phases in the direction perpendicular to it. Long arrows indicate significant departure from one–dimensionality (1-D), whereas short arrows indicate that the Earth below is relatively uniform laterally within the sensing region of the site at those periods. An absence of an arrow, for instance east of Yellowknife at frequencies of 1 to 0.1 Hz (Fig. 10-3d), indicates that the phase difference is statistical insignificant, and infers a 1-D subsurface at the depths being sensed by that frequency bin.

At high frequencies (above 1 Hz, Fig. 10-3a,b,c), where penetration into the subsurface is in the order of a few kilometres, there is significant site-to-site variability. This is an expression of the 3-D nature of the near-surface geology. Note that the longest arrows, which represent the largest phase difference and therefore are indicative of the greatest lateral variability, occur in the vicinity of the Yellowknife River Fault Zone, especially at frequencies of 10 to 0.1 Hz, and are parallel to the brittle West Bay Fault System. At frequencies below 0.1 Hz (Fig. 10-3e,f), at which the EM waves are penetrating some 20 km into the crust, the geoelectric strike direction is uniform across the region with a best-fit direction of ~025º.

Figure 10-4 shows the best strike directions fitting all sites simultaneously with sliding frequency windows of varying widths, 1/6, 1/3, 1/2 of a decade, and 1, 2, and 3 decades wide. The overall best-fitting geoelectric strike

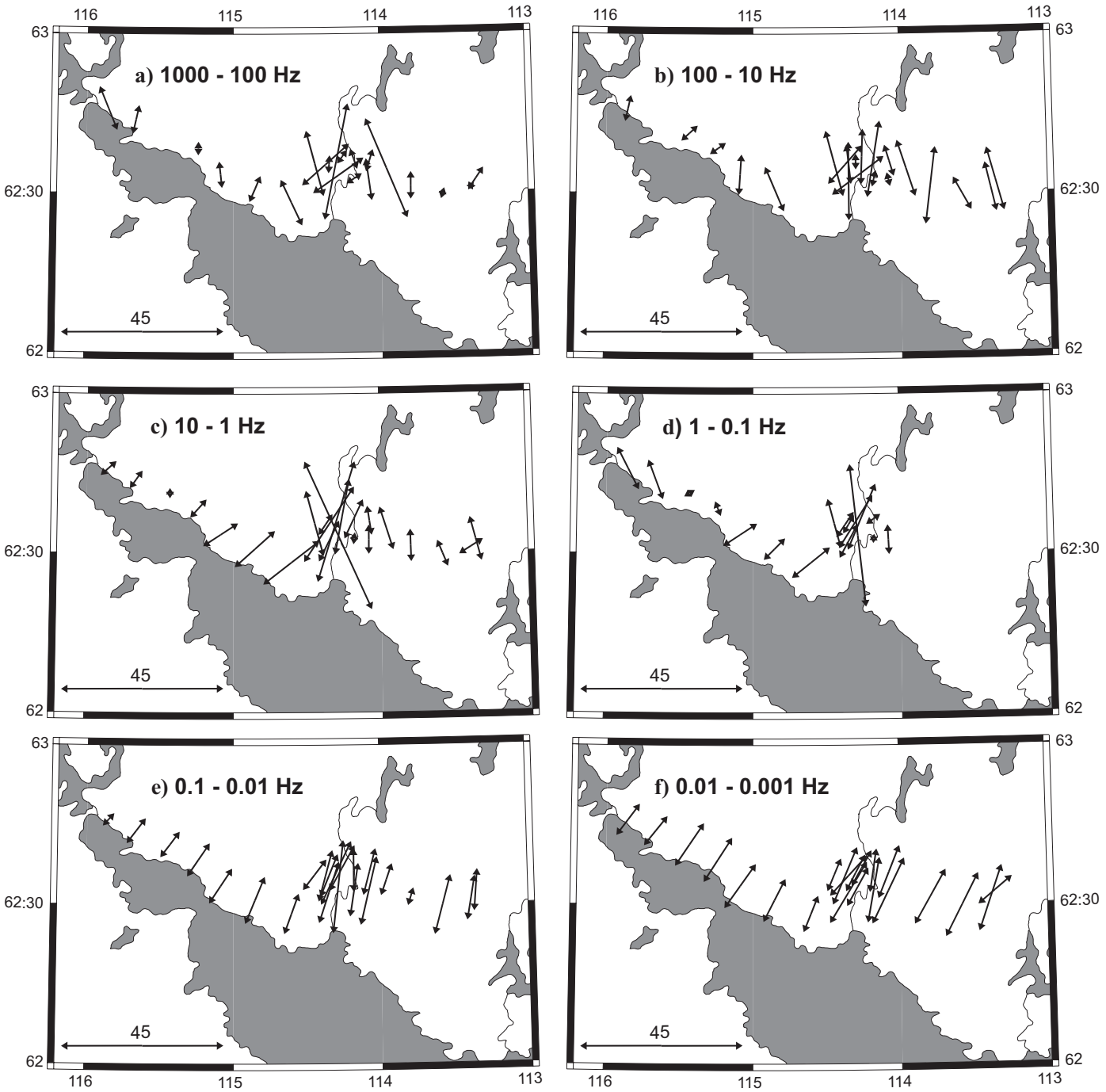

Figure 10-3. Geoelectric strike directions at each site in the decade-wide frequency bands. The length of the arrow is representative of the phase difference in the strike direction and perpendicular to the strike direction, and therefore is an indicator of dimensionality. A 45º-phase difference arrow is shown in the lower left-hand corner of each plot.

direction displays a frequency dependence, with high frequencies exhibiting a preference for ~000º (north-south), and low frequencies exhibiting a preference for ~025º. The change occurs at frequencies of around 10 to 1 Hz, at which the EM waves are penetrating on average some 2 to 6 km.

Given that the focus of this study is the upper and middle crust, the appropriate interpretation coordinate reference frame to choose is the one that is consistent with the high-frequency data that penetrate from the surface to about 20 km depth. For these data, those depths correspond to frequencies in the range of 1,000 to 0.1 Hz. The higher frequency data are excluded as they are not as good quality and do not exist for all sites. The best-fitting overall strike direction from all 22 sites in the frequency range of 1,000 to 0.1 Hz is ~001.5º, or north-south. The eight sites along the high-resolution profile indicate a preference for a strike of ~012º, but a north-south strike yields only a 14% worse misfit with most of the misfit at the lower frequencies (1–0.1 Hz). Accordingly, the regional interpretation coordinate reference frame was taken to be north-south and east-west. In this reference frame, the currents flowing north-south represent the TE-mode of induction, and those flowing east-west represent the TM-mode.

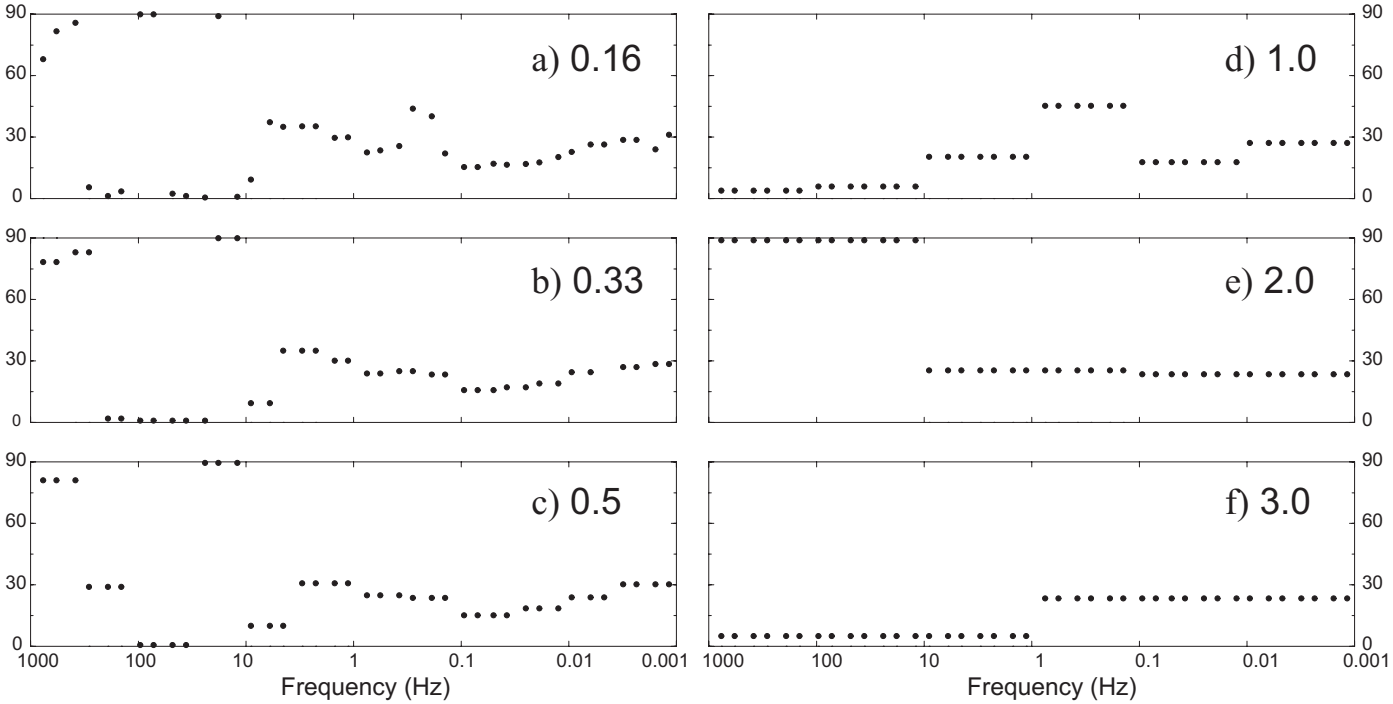

Figure 10-4. Geoelectric strikes for all 22 sites simultaneously for frequency bands of widths varying from 1/6th of a decade **(a)** to 3 decades **(f)**.

Usually, one fits the observations to a model including distortion to extract the best estimates of the regional MT impedances in the regional interpretation coordinate reference frame (see, e.g., Groom et al., 1993; Jones and Dumas, 1993). Rotation of the data into strike direction is less preferred as it usually results in poorer estimates of the regional responses (see, e.g., Jones and Groom, 1993; McNeice and Jones, 2001). However, the data collected on this survey display unusually low galvanic-distortion effects. For these data, twist and shear values are below 15º for most sites, or low distortion effects, indicative of little near-surface conductive heterogeneity. This is to be compared with high-distortion effects, with values close to the physical limits of 60º and 45º respectively, more typically seen in Archean terranes. Accordingly, for these data simple rotation into the interpretation coordinate system suffices.

Prior to plotting and modelling, the data were visually inspected and obvious outliers and problem data were eliminated. The usable frequency range for modelling at each site is listed in Table 10-1.

DATA PLOTS

Magnetotelluric Pseudosections

Plots of the regional MT data are shown in Figure 10-C5 as contoured pseudosections. The hotter colours (yellows and reds) in the sections indicate low resistivities (in the apparent resistivity sections) and high phases (in the phase sections), both indicative of the presence of conductivity anomalies. The data have been edited to remove obvious outliers and distortions, and the data from site 105 are excluded due to their anomalous behaviour (see below). Where acceptable data exist, they are shown by dots on the sections. Areas where data do not exist are contouring interpolations and should not be considered for interpretation.

The apparent resistivity sections (Fig. 10-C5a,c) show low resistivities in the region around Yellowknife and sites to the east, which are an indication of conducting structures below those locations. The low apparent resistivities persist

Table 10-1. MT stations along the regional and high-resolution profiles.

Station	Year	Latitude	Longitude	Equipment	Freq. Range (Hz)	Vertical magnetic
Regional Profile						
003	1996	62°45'55	115°51'14	V5 + LiMS	768 – 0.000147	Y
004	1996	62°43'51	115°39'50	V5 + LiMS	768 – 0.000147	Y
006	1996	62°41'17	115°25'58	V5 + LiMS	768 – 0.000147	Y
007	1996	62°38'26	115°14'20	V5 + LiMS	768 – 0.000147	Y
008	1996	62°33'30	115°05'16	V5 + LiMS	768 – 0.000147	Y
009	1996	62°30'50	114°51'10	V5 + LiMS	768 – 0.000293	Y
005	1996	62°28'13	114°36'22	V5	10,000 – 0.00110	Y
010	1996	62°32'15	114°21'03	V5 + LiMS	768 – 0.000293	Y
045	2000	62°33'17	114°17'13	GMS-06	193 – 0.000336	N
033	1999	62°32'43	114°10'47	V5-2000	288 – 0.000550	N
011	1996	62°32'30	114°04'48	V5 + LiMS	768 – 0.000293	Y
012	1996	62°31'18	113°47'45	V5 + LiMS	10,000 – 0.000293	Y
013	1996	62°29'44	113°34'51	V5 + LiMS	768 – 0.000147	Y
014	1996	62°30'57	113°23'12	V5	10,000 – 0.00110	Y
High resolution profile						
101	2000	62°35'36.3	114°26'44.2	GMS-06	209 – 0.000641	N
102	2000	62°35'23.2	114°22'25.8	GMS-06	193 – 0.000336	N
103	2000	62°35'23.2	114°20'54.7	GMS-06	193 – 0.000336	N
104	2000	62°35'55.7	114°18'07.2	GMS-06	193 – 0.000336	N
105	2000	62°36'49.2	114°15'34.7	GMS-06	193 – 0.000336	N
106	2000	62°36'23.9	114°10'55.9	GMS-06	150 – 0.000641	N
107	2000	62°36'06.1	114°04'29.5	GMS-06	193 – 0.000336	N
032	1999	62°34'37	113°57'36	V5-2000	288 – 0.00110	N

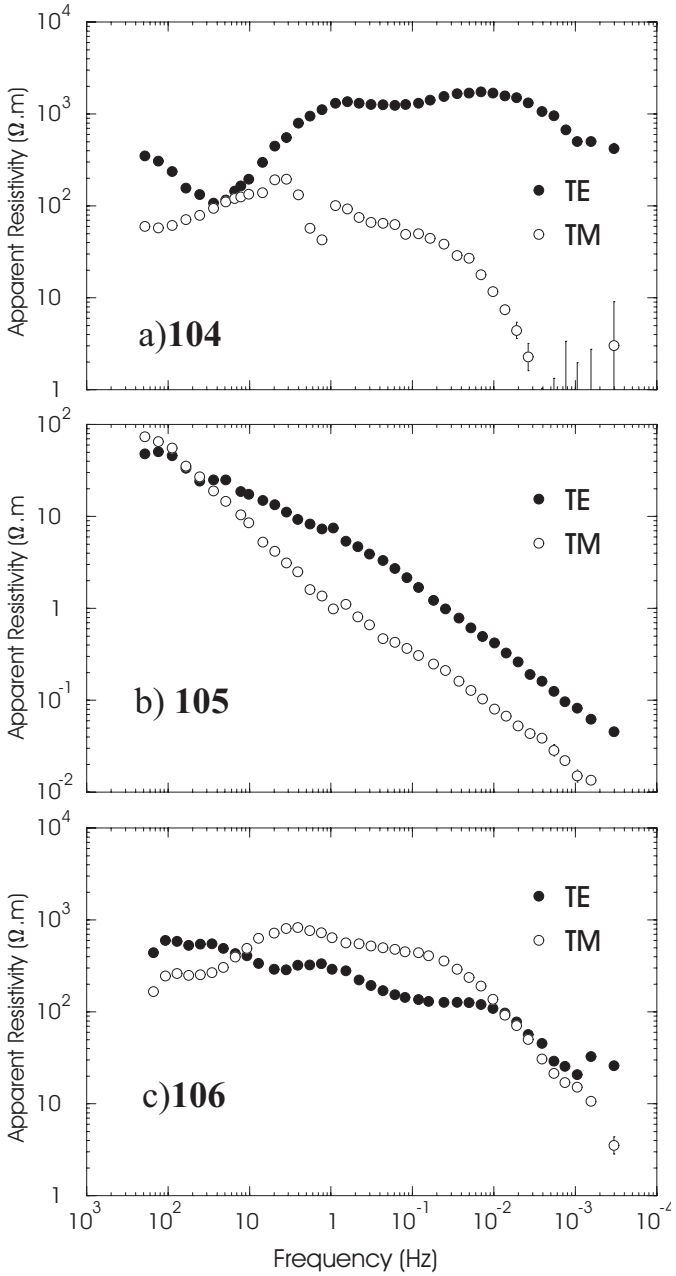

Figure 10-6. MT apparent resistivity curves for the three EXTECH III sites crossing the Yellowknife Fault, sites 104, 105, and 106. Note that the data for site 105 is on a different scale from the other two. The full symbols are those for the TE-mode, and the open symbols are those for the TM-mode. The solid bars indicate one standard error; where omitted, the error is smaller than the plotting symbol.

to the lowest frequencies, suggestive of structures with whole crustal extent and possibly penetrating into the uppermost mantle.

Site 105 Response

Site 105 exhibits the strongest and most anomalous MT response of the whole data set, and the data were excluded from Figure 10-C5 so as not to bias the plots. Figure 10-6 shows the apparent resistivity curves from site 105 (Fig. 10-6b), plus those from the neighbouring sites 104 (Fig. 10-6a) and 106 (Fig. 10-6c). The data are plotted in terms of log frequency along the abscissa, with frequency decreasing to the right, and decreasing frequency is a proxy for increasing depth. Note that the log apparent resistivity scale (along the ordinate) for site 105 is different from that of the other two sites.

Site 104 shows strong two-dimensionality, with the TE-mode data higher in amplitude than the TM-mode data. This is indicative of a site on the conductive side of a fault. The data at site 106 are more one-dimensional and remain moderately resistive until 0.01 Hz or so. In sharp contrast the apparent resistivity data at site 105 drop sharply and continuously with decreasing frequency. The two curves are almost together, indicating a 1-D Earth below as far as the MT data are probing; modelling of these data is discussed below.

Given that the high-frequency apparent resistivity data at sites 104 and 106 asymptote to a few hundred ohm.metres (150 and 270 Ω.m respectively), and for site 105 is 60 Ω.m, then there is a possible static shift in the data from site 105 of 3 to 5. This translates to a possible multiplicative error in depth of 1.7 to 2.4 (square root of apparent resistivity shift, see Jones, 1988), i.e., the depths to interfaces must be multiplied by 1.7 to 2.4.

Induction Vectors and Geomagnetic Transfer Functions

Real induction vectors for the four sites on either side of the Yellowknife River Fault Zone are shown at 10 Hz, the frequency of greatest response at site 010, in Figure 10-7a. The figure shows the classic induction vector reversal (e.g., Jones et al., 1992); vectors at sites 005 and 010 point eastwards, whereas the vectors at sites 011 and 012 point westwards. When resolved along an east-west section, the real and imaginary GTFs at 10 Hz for those four sites are as shown in Figure 10-7b. Both real and imaginary vectors exhibit the strong reversal, and the crossovers (from east pointing for the western sites to west pointing for the eastern sites) are well defined in the vicinity of site 105. This site is situated virtually on top of the Walsh Lake Formation (Fig. 10-2). These vectors and GTFs are indicative of current flow in a relatively linear (i.e., 2-D) upper crustal conductor between sites 010 and 011.

MODELLING AND INVERSION

One-Dimensional Modelling of Site 105 Response

The MT data from site 105 (Fig. 10-6b) are highly unusual in that even the lowest frequencies do not penetrate through the shallow, subsurface conductor, and that the conductor is increasing in electrical conductivity with depth. The data can be modelled using one-dimensional (1-D) approaches given that both modes (TE and TM) show almost identical apparent resistivity curves. The data modelled were the so-called Berdichevsky averaged data (Berdichevsky and Dmitriev, 1976), which are the rotationally invariant arithmetic means of the TE and TM impedances, and error floors of one degree in phase and 3.5% in apparent resistivity were set. Analysis with Parker's D^+ (Parker, 1980; Parker and Whaler, 1981), and using Schmucker's C-function (Schmucker, 1970), which gives the depth to maximum eddy current flow (Weidelt, 1972), shows that the maximum depth of penetra-

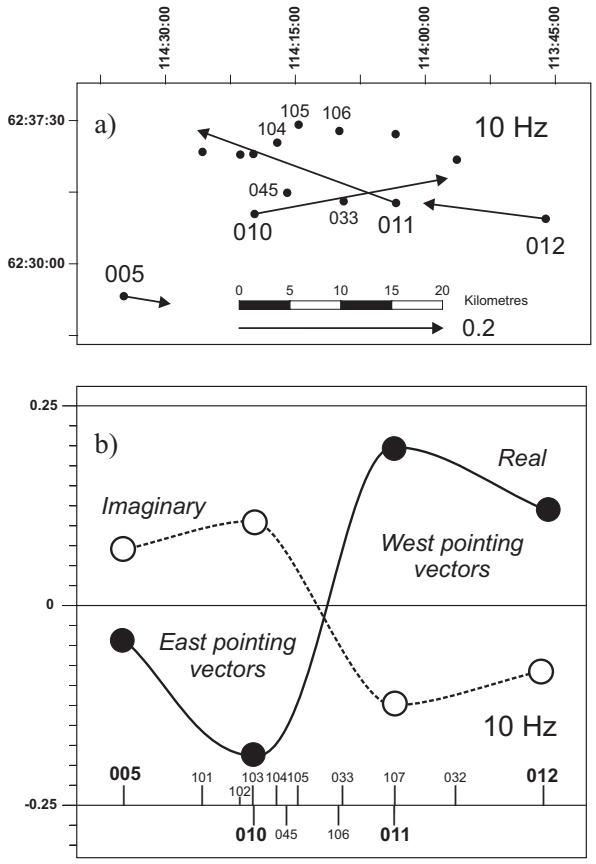

Figure 10-7. **(a)** Real (reversed) induction vectors from sites in the vicinity of the Yellowknife Fault. Vertical magnetic field data were only acquired at the four sites shown. **(b)** East-west geomagnetic transfer functions at the four sites close to the Yellowknife Fault. Note the strong crossovers in both the real and imaginary parts inferring current concentration in an anomalous body close to site 105.

tion is to about 2,500 m, even at 0.001 Hz frequency (1,000 s period). This is to be compared to neighbouring sites 104 and 106, where the EM fields at 0.001 Hz frequency are flowing at depths of around 50 km. At site 105 the EM fields are arrested in the very high conductivity anomaly and cannot penetrate through it. The two highest frequency and three lowest frequency data are omitted from the inversion because of their large error estimates and inconsistency with the other data.

Modelling was accomplished using two different inversion strategies that result in models with least structure, where least-structure is defined either by the minimum number of layers or the minimum change between layer resistivities. The model with the minimum number of horizontal layers that fits the data was determined by increasing the number of layers until the data fit with a normalized root mean square (RMS) misfit of 1.0, i.e., the difference between the observed data and the modelled data is, on average, one standard error. An RMS of 1.0 is the goal of any model fitting. A smaller value infers that the data are being over fit, and a larger value, that the data are not being sufficiently fit. This was achieved with 6 layers using the codes of Fischer et al. (1981) and Fischer and Le Quang (1981). Best-fitting models with four or five layers gave an RMS of 2.5 or greater, whereas models with six or more layers could be found with an RMS of 1.0 or less. The parameters of the best-fitting six-layer model are given in Table 10-2, and the model and fit are shown in Figure 10-8.

Table 10-2. Parameters of the best-fitting six-layer model to site 105 averaged MT data.

Layer	Resistivity (Ω.m)	Range (Ω.m)	Depth to base (m)	Thickness (m)	Range (m)
1	45	18 - 120	86.6	86.6	16.9 - 445
2	690	69 - 6900	233	147	60.1 - 352
3	2.7	2.3 – 3.1	467	234	210 - 259
4	0.62	0.48 – 0.79	1030	561	457 - 688
5	0.05	0.027 – 0.10	1800	775	415 - 1450
6	0.005	0.00065 – 0.040			

Having found an acceptable model, the next step is to appraise it for resolution of the model parameters. Model resolution was investigated using a linearized approach (singular value decomposition, SVD, Wiggins, 1972; Edwards et al., 1981; Jones, 1982), and standard errors on the model parameters are also listed in Table 10-2. The SVD analysis shows that of the eleven model parameters, eight are well determined, two are marginally determined (ρ_6, resistivity of lowermost layer, and h_1, thickness of top layer), and one is undetermined (ρ_2, resistivity of second layer). The latter is a well-known problem in MT, whereby the resistivity of a resistive layer sandwiched between two conductive ones is virtually impossible to determine, even with precise data (e.g., Jones, 1999, for a discussion of this). At best, one can determine the minimum value for the resistive layer.

The second approach was to determine the smoothest model, defined as the one with the least total resistivity gradient, or change between layers. Using the Occam algorithm of Constable et al. (1987), a model of 350 layers fitting the data to an RMS of 1.0, which simultaneously had a minimum in roughness (sum of resistivity gradients), was determined and it is shown in Figure 10-8 together with the fit to the data.

Both the minimum-layers model and the smoothest model show essentially the same subsurface structure to a few kilometres. The layers in the layered model are well rep-

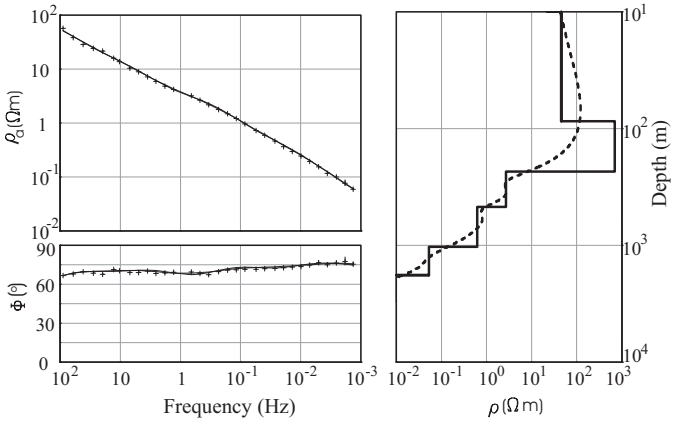

Figure 10-8. One-dimensional models of the averaged MT data for site 105.

resented by maxima and minima in the smooth model. The top 100 m is moderately resistive, below which is a resistive zone to some 250 m or so. Beneath that is a conducting region with decreasing resistivity with depth to extraordinary low values at depths of 1 km and deeper.

The MT data do not penetrate through this conducting region. The phases at the lowest frequencies (0.001 Hz) are still high (75º) and are not dropping back down to 45º, which would indicate penetration through the body. Similarly, the apparent resistivity curves are not beginning to trend upwards at the lowest frequency.

Note that because of the possibility of the apparent resistivity curves being static shifted downwards, the depths in the 1-D models may be systematically underestimated by a multiplicative factor of possibly 1.7 to 2.4 (see above), and resistivities can be greater by a factor of 3 to 5. Thus, the top of the conducting layer could be as deep as 560 m, rather than 233 m. Further AMT data need to be acquired, with some control over static shift, in order to obtain a more accurate estimate. This anomalous highly conducting body below site 105 is the likely explanation for the 10 Hz induction vectors, shown in Figure 10-7.

Two-Dimensional Modelling

The MT and GTF data in the regional coordinate reference frame were modelled to obtain the subsurface 2-D electrical resistivity structure using the objective inversion procedure of Rodi and Mackie (2001), as implemented within Geosystem's WinGLink© software package. The inversion scheme tries to fit the data as well as possible, whilst simultaneously finding the smoothest model at the prescribed level of misfit. Smoothness is defined by the sum of the horizontal and vertical gradients in resistivity, so the smoothest model possible is a uniform Earth.

Models were derived using 17 of the 22 sites, illuminating both the regional crustal and lithospheric mantle structures, and local structures within and around the Yellowknife River Fault Zone. The responses from site 105 were excluded as they only penetrate to a few kilometres and would require excessive gridding in the vicinity of the site to ensure accurate modelling. Additionally, the data from sites 010, 045, 033, and 011 were excluded as they duplicate data from sites on the high-resolution profile.

To account for the anisotropic part of "static shifts" (Jones, 1988), which are multiplicative shifts of the apparent resistivity curves caused by local, near-surface inhomogeneities, the apparent resistivity curves were coalesced at their high-frequency asymptotes. The split between the two curves were, in most cases, minor and less than half a decade. To account for the final local site gains, the apparent resistivities were set with an error "floor" of 7% (equivalent to 2° in phase) whereas the phase data were set with an error floor of 1° (equivalent to 3.5% in apparent resistivity). The error floor for the GTFs was set at 0.05 absolute. Error floors perform the task of specifying the minimum error for each data point. If the errors are smaller than the respective floors, then they are set to the floor value. If they are larger, then the true error is taken. Surprisingly, as discussed above, these data were little perturbed by local distortions, so we could set a low error floor for the apparent resistivities. Typically, error floors are set at far larger values.

The MT data from all 22 sites, and GTF data from 12 sites (see Table 10-1), in the frequency range 1000 to 0.001 Hz (6 decades of frequency), were available for inversion for regional structure. Two models were derived, one from the MT data alone, fitting both the TE and TM modes simultaneously, and one from the MT data and GTF data together. These two models are shown in Figure 10-C9, and in Figure 10-C10 the data and the model responses for the TE+TM model are compared. In both cases, the start model was a uniform half-space with a resistivity of 1,000 Ω.m, and many hundreds of iterations were performed. Both models fit the data well at crustal and upper mantle probing frequencies. The misfit is predominantly at the lowest frequencies (see Fig. 10-C10), but penetration at these frequencies is over 100 km, which is beyond the scope of this paper. The models were derived without any a priori constraints being applied, such as horizontal or vertical discontinuities or boundaries. The two models show virtually identical crustal and upper mantle resistivity structures for the YRFZ and the region as a whole. Differences between the two models are suspect and are not discussed. Below the TE+TM model is compared with other data preferentially over the TE+TM+GTF model due to its superior fit.

DISCUSSION

Crustal Resistivity

The crust in the southwestern part of the Slave craton, apart from the top kilometre or so and the region of the Yellowknife River Fault Zone, is highly resistive with values well in excess of 10,000 Ω.m. Such high resistivities are consistent with those obtained from laboratory studies of dry crustal rocks (Olhoeft, 1981; Laštovicková, 1991) for the expected pressure-temperature conditions. However, beneath most other parts of continental crust the lower crust is typically orders of magnitude less resistive, leading to speculations for the enhanced conductivity ranging from saline fluids to carbon on grain boundaries (see review by Jones, 1992). When this lack of a regional lower crustal conductor was first reported (Jones and Ferguson, 2001) it was the only occurrence known, although local anomalously resistive zones had been previously reported (e.g., Park and Mackie, 2000). Since then, other regions have shown such high resistivities throughout the crust, notably east of the Great Slave Lake shear zone at the southern boundary of the Slave craton (Wu et al., 2002), and the Archean Rae craton at the Rae-Hearne boundary near Baker Lake (Jones et al., 2002).

Whereas the existence of a lower crustal conducting layer is powerful information, though it is plagued by questions about the cause of the enhanced conductivity (Jones, 1992; Yardley and Valley, 1997; Wannamaker, 1997), the lack of any conductor is just as powerful in that any conducting mechanism, such as deep crustal conducting metasediments, must be excluded from the tectonic scenario model. Note that the locations of resistive crust are all Archean in age, and likely Mesoarchean or earlier (see cross-section in Bleeker, 2002). Given that continental crust of ages younger than Mesoarchean predominantly displays a conducting lower

crust, with a possible age relationship (e.g., Jones, 1981, 1992; Hyndman and Shearer, 1989), the obvious implication is that processes that resulted in subducted sediments were not as efficient in the Mesoarchean and earlier. This in turn suggests that modern-day plate tectonics, *sensu stricto*, was not the dominant tectonic process when the Central Slave Basement Complex was formed.

Yellowknife River Fault Zone

The class of models shown in Figure 10-C9 are minimum structure, which means that the Yellowknife River Fault Zone can be narrower and more conducting, but not wider and more resistive. Within the Yellowknife River Fault Zone, resistivities are reduced to low values (1000 Ω.m or less) to depths of at least 20 km, and possibly through the whole crust (Fig. 10-C9). There is also reduced resistivity in the upper mantle beneath the fault and to the east (Fig. 10-C9). The clear implication from the MT data is that the Yellowknife River Fault Zone, and/or coincident Proterozoic brittle faults of the West Bay-Indin Lake Fault System (e.g., Bleeker, 2002), extend through the whole crust. This contrasts with the Rocky Mountain Trench-Tintina Fault (Ledo et al., 2002), the Great Slave Lake shear zone (Wu et al., 2002), and the San Andreas Fault (Mackie et al., 1997), which all exhibit higher resistivities in the fault. In contrast, the Fraser Fault (Jones et al., 1992) and the Great Glen Fault (Kirkwood et al., 1981) exhibit reduced resistivity in the fault zone. What causes these differences is an open question, and likely related to fluid and rheological processes.

Yellowknife Basin

The depth extent and geometry of the Yellowknife basin is contentious, with Cook et al. (1999) and van der Velden and Cook (2002) arguing that it is about 7 km in the east (near Tibbit Lake), shallowing to the west towards the Yellowknife Fault (Fig. 10-C11). In contrast, Bleeker (2002) and Snyder et al. (2006) argue that the basin is defined by a prominent reflector (Y2, see Fig. 10-C11) marking a regionally-significant unconformity between the Central Slave Basement Complex felsic rocks and granitoids, and the overlying quartzite, banded iron formation, and mafic/ultramafic rocks of the Central Slave Cover Group (Bleeker et al., 1999a) that lies unconformably on the Central Slave Basement Complex (Bleeker et al., 1999a,b).

The moderately resistive region to the east of Yellowknife in the two models is likely due to the metasedimentary rocks of the Yellowknife Supergroup. There are two conductive candidates, the banded iron formation that lies at the top of the Central Slave Cover Group and black (graphitic) argillite of the Walsh Lake Formation, stratigraphically immediately below the Burwash Formation. The implication from the MT models is that the Yellowknife Basin does have a significant depth extent close to Yellowknife, and thus supports the interpretation of Bleeker (2002) and Snyder et al. (2006). More discussion of this is given below.

Correlation with Other Geophysics

Both seismic reflection and seismic refraction profiles were undertaken along the all-weather road from Rae to Tibbit Lake as part of LITHOPROBE SNORCLE transect studies. The road follows the locations of MT sites 003 – 004 – 006 – 007 – 008 – 009 – 005 – 010 – 011 – 012 – 013 – 014. The seismic reflection interpretation is presented in Cook et al. (1999), and re-interpretations by van der Velden and Cook (2002) and Snyder et al. (2006). The migrated seismic data, together with the interpretation of van der Velden and Cook (2002), are shown in Figure 10-C11 and are compared to the TE+TM resistivity model of Figure 10-C9a (note that the resistivity model has been differentially stretched to compensate for the trajectory of the roads on which the reflection data were acquired).

Note the general observation of higher reflectivity in resistive regions, an observation that is common within LITHOPROBE data sets (e.g., Clowes et al., 1999). The lower resistivities within the fault zone generally correlate with an absence of reflectivity, and in detail with the westernmost extent of reflector Y2, interpreted as a fault by van der Velden and Cook (2002) and as the Central Slave Cover Group by Bleeker (2002) and Snyder et al. (2006). Although we subscribe to the view of Snyder et al. (2006) that reflector Y2 is likely truncated by the Yellowknife River Fault Zone rather than correlative with reflector A3 to the west of Yellowknife, as proposed by van der Velden and Cook (2002), given the ubiquitous presence of the banded iron formation in the Central Slave Cover Group, which should provide an excellent conductive target, we do not support the notion that Y2 represents the Central Slave Cover Group. Rather, we submit that the geometry of the basin is well described by the resistivity model with a maximum thickness of about 10 km beneath site 032 some 20 km to the east of Yellowknife, and shallowing to between 2 and 3 km further east and west.

The SNORCLE seismic refraction experiment is described, and the data interpreted, in a recent paper by Fernández Viejo and Clowes (2003). Their compressional wave velocity model for the Rae to Tibbit Lake profile is shown in Figure 10-C12a. Shot point 1102 was at the Yellowknife Con mine. The solid lines on Figures 10-C12a and 10-C12b are interfaces from which wide-angle reflections were observed, and the dashed lines denote the progressively linearly increasing velocity at 0.2 km/s intervals. In contrast to the teleseismic observations, which suggested a Moho at a depth of some 39 km beneath the Yellowknife seismic array (Bank et al., 2000), seismic refraction Moho is observed at 33 km beneath the southwestern part of the craton. The dominant feature of the refraction model is the lower velocities observed to the east of Yellowknife compared to the west. The lower crustal velocity to the east ranges from 6.5 to 6.7 km/s, whereas to the west it is 6.6 to 6.9 km/s.

A comparison of the reflection model and wide-angle reflectors with the resistivity model is given in Figure 10-C12b. The lower velocities in the lower crust to the east of Yellowknife compared to the west correlate with the lower resistivities observed for that region, although this is a weakly resolved feature of the resistivity model.

Causes of Conductivity Enhancement

Outside the Yellowknife River Fault Zone itself, formations that are probable candidates for enhancing electrical conductivity are the banded iron formation, which lies at the top of

the Central Slave Cover Group, and the black (graphitic/sulphitic) argillite of the Walsh Lake Formation (see above). Thus we can conclude that within the Yellowknife Basin the likely cause of conductivity enhancement is due to iron oxides (sulphides) or graphite.

Within the fault zone itself, laboratory physical property studies have been undertaken by Scromeda et al. (2000), Connell et al. (2001), Connell and Scromeda-Perez (2002), and Katsube et al. (2006) of rocks from the Giant and Con mines. They demonstrate that the rocks at the surface display strong electrical anisotropy, with layers of relatively high concentrated sulphide (>10%) in one gold-bearing sample showing a resistivity of 10 to 100 Ω.m parallel to foliation and more than an order of magnitude higher perpendicular to foliation. The relatively high values of 10 to 100 Ω.m for sulphide ore are explained by Connell et al. (2001) as due to the lack of grain-to-grain connectivity. By induction, we conclude that the broad moderately conducting fault zone to middle and lower crustal depths is caused by sulphide mineralization. Laboratory measurements show that pyrite sulphides can have a range in resistivity from 10^{-7} to 1 Ω.m, with an average of 10^{-2} Ω.m (Beblo, 1982), and therefore a well connected sulphide body should exhibit resistivities orders of magnitude below those observed. An alternative explanation would be in terms of fluids within the brittle faults. However, we exclude this using the same arguments as Gough (1986), who explained the often observed seismically transparent and resistive upper crust, when compared with the reflective and conductive lower crust, in terms of rheological state.

The astounding anomaly beneath site 105 is likely to be the graphitic argillites of the Walsh Lake Formation, or conversely may be interconnected sulphides.

CONCLUSIONS

A magnetotelluric study was performed along a short profile crossing the Yellowknife River Fault Zone as a contribution to EXTECH III activities. The data from this study, taken together with regional MT data acquired by LITHOPROBE for SNORCLE transect investigations of the Slave craton, yield information about the subsurface geometries of resistivity structures. Strike analysis demonstrated that much of the data can be regarded as one-dimensional, and that two-dimensional structures generally strike north-south, and such a coordinate reference frame was adopted for interpretation.

The MT data from site 105 are virtually one-dimensional, and are indicative of a highly conducting body at a depth of some 250 m, with increasing conductivity (decreasing resistivity) with depth. One caution is that this is a single station anomaly, and it requires verification through a more detailed survey with MT stations "nose-to-nose", i.e., continuous MT sites with site spacing the same as the electrode line length (50–100 m), such as was undertaken by Poll et al. (1987) over the Leitrim Fault near Ottawa and Unsworth et al. (1997, 1999) over the San Andreas Fault in California. Site 105 is some 2750 m northeast from site 104, and some 4000 m west-northwest from site 106, and modelling studies suggest that the anomalous body at 250 m and below must be of limited spatial extent (likely <500 m) otherwise it would have a measurable effect on the MT data from sites 104 and 106. A grid of MT sites, with some sort of static shift control, would be able to ascertain the lateral boundaries of the body.

Two-dimensional objective inversion modelling of 17 sites, from the 22 available sites, resulted in models that showed regional-scale features correlative with geology and seismology. The MT models do not support the Yellowknife Basin interpretation of van der Velden and Cook (2002), but neither do they support the interpretation of Bleeker (2002), and repeated in Snyder et al. (2006). The MT models suggest a basin geometry that is shallow in the eastern half of the Ingraham Trail and deepening to 10 km in the western half.

Electrically, the Yellowknife River Fault Zone penetrates the whole crust, and there is reduced resistivity in the lithospheric mantle beneath it. Given the high resistivities observed throughout the whole crust on either side of the fault zone, the implication is that mantle fluids, which provided the source of the gold mineralization, came directly along a vertical path. The importance of such a structure is readily apparent when the distribution of gold showings in the southern Slave Province is displayed on a map. The densest concentration of showings and the most economically significant ones are focused along the western margin of the Yellowknife Basin in an arc from Yellowknife to Nicholas Lake in a fashion reminiscent of other well known structures, such as the Cadillac-Larder Lake Break in the Abitibi Province of the Canadian Shield.

ACKNOWLEDGMENTS

Many people contributed significantly to acquiring the MT data reported in this paper. George Elliot led the Phoenix Geophysics crew that acquired the 1996 AMT and BBMT data. Gary McNeice, initially of Phoenix Geophysics and later Geosystem Canada, led the crews responsible for the acquisition of all the other AMT and BBMT data. Nick Grant, now in Vancouver, was responsible for the LMT data acquired in 1996. Phoenix Geophysics, especially Leo Fox, is particularly thanked for allowing us to use their newly developed V5-2000 systems on the 1998 winter-road survey — the first ever commercial survey with those new generation instruments.

The winter-road surveys around Yellowknife were made possible through the generous logistical support of Royal Oak Mines (then owners of the Giant mine) and Miramar Con Mine Ltd., and through generous donations of time by the staff of the Yellowknife Seismic Observatory and at the CS Lord Northern Geoscience Centre. The authors want in particular to acknowledge Hendrik Falck, of C.S. Lord, who spent many hours and days aiding and abetting our efforts. We could not have accomplished as much as we did without Hendrik's support.

Hendrik Falck also supplied the geology map in Figure 10-1, and provided significant input to the geological description and to early versions of this manuscript. Arie van der Velden is thanked for supplying the seismology data and interpretation in Figure 10-C11. Wouter Bleeker provided substantial comments, and Kevin Stevens and an unknown reviewer gave useful suggestions for improving the submitted version.

LITHOPROBE publication number 1370. Dublin Institute for Advanced Studies publication number GP169.

REFERENCES

Andersen, F., Boerner, D.B., Harding, K., Jones, A.G., Kurtz, R.D., Parmelee, J., and Trigg, D.
1988: LIMS: Long period intelligent magnetotelluric system; 9th Workshop on EM Induction, Sochi, USSR, October 24 - 31.

Bahr, K.
1984: Elimination of local 3D distortion of the magnetotelluric tensor impedance allowing for two different phases; Seventh Workshop, Electromagnetic Induction in the Earth and Moon, IleIfe, Nigeria, August 15-22.
1988: Interpretation of the magnetotelluric impedance tensor: Regional induction and local telluric distortion; Journal of Geophysics, v. 62, p. 119-127.
1991 Geological noise in magnetotelluric data: A classification of distortion types; Physics of the Earth and Planetary Interiors, v. 66, p. 24-38.

Bailey, G.
1987: A guide to the Shot Member of the Banting Group, Yellowknife volcanic belt; *in* Yellowknife Guide Book: A Guide to the Geology of the Yellowknife Volcanic Belt and Its Bordering Rocks, (ed.) W.A. Padgham; Geological Association of Canada, Mineral Deposits Division, Yellowknife, NWT, Canada, p. 81-87.

Bailey, R.C. and Groom, R.W.
1987: Decomposition of the magnetotelluric impedance tensor which is useful in the presence of channeling; 57th Annual International Society of Exploration Geophysicists Meeting and Exposition, Expanded abstracts, Tulsa, OK, v. 57, p. 154-156.

Bank, C.-G., Bostock, M.G., Ellis, R.M., and Cassidy, J.F.
2000: A reconnaissance teleseismic study of the upper mantle and transition zone beneath the Archean Slave craton in NW Canada; Tectonophysics, v. 319, p. 151-166.

Beblo, M.
1982: Electrical conductivity of minerals and rocks at ordinary temperatures and pressures; *in* Numerical Data and Functional Relationships in Science and Technology; Group V: Geophysics and Space Research, Volume 1: Physical Properties of Rocks. Chapter 5.1, p. 239-253.

Berdichevsky, M.N. and Dmitriev, V.I.
1976: Basic principles of interpretation of magnetotelluric sounding curves; *in* Geoelectric and Geothermal Studies, (ed.) A. Ádám; KAPG Geophysical Monograph, Akademiai Kiad, Budapest, p. 165-221.

Bleeker, W.
2002: Archean tectonics: A review, with illustrations from the Slave craton; *in* The Early Earth: Physical, Chemical and Biological Development, (ed.) C.M.R. Fowler, C.J. Ebinger, and C. J. Hawkesworth; The Geological Society of London, Special Publication Number 199, p. 151-181.

Bleeker, W. and Ketchum, J.W.F.
1998: Central Slave basement complex, Northwest Territories; Its autochthonous cover, décollement, and structural topology; Geological Survey of Canada, Current Research, p. 9-19.

Bleeker, W., Ketchum, J.W.F., and Davis, W.J.
1999a: The Central Slave Basement Complex, Part II: Age and tectonic significance of high-strain zones along the basement-cover contact; Canadian Journal of Earth Sciences, v. 36, p. 1111-1130.

Bleeker, W., Ketchum, J.W.F., Jackson, V.A., and Villeneuve, M.E.
1999b: The Central Slave Basement Complex, Part I: Its structural topology and autochthonous cover; Canadian Journal of Earth Sciences, v. 36, p. 1083-1109.

Cagniard, L.
1953: Basic theory of the magnetotelluric method of geophysical prospecting; Geophysics, v. 18, p.605-635. Reprinted in Vozoff (1986), p. 4-34.

Chakridi, R., Chouteau, M., and Mareschal, M.
1992: A simple technique for analysing and partly removing galvanic distortion from the magnetotelluric impedance tensor: Application to Abitibi and Kapuskasing data (Canada); Geophysical Journal, v. 108, p. 917-929.

Clowes, R.M.,Cook, F.A., Hajnal, Z., Hall, J., Lewry, J., Lucas, S., and Wardle, R.
1999: Canada's LITHOPROBE project (collaborative, multidisciplinary geoscience research) leads to new understanding of continental evolution; Episodes, v. 22, p. 3-20.

Connell, S., Katsube, T.J., Hunt, P., and Kerswill, J.
2001: Electrical Mechanism of Mineralized Rocks from Giant And Con Mine Areas, Northwest Territories; Geological Survey of Canada Current Research, 2001-C2, 10 p.

Connell, S. and Scromeda-Perez, N.
2002: Electrical Conductivity Mechanism of Sericite Schist from Gold Lake Area of the Yellowknife Mining District, Northwest Territories; Geological Survey of Canada, Current Research, 2002-C5, 6 p.

Constable, S.C., Parker, R.L., and Constable, C.G.
1987: Occam's inversion: a practical algorithm for generating smooth models from electromagnetic sounding data; Geophysics, v. 52, p. 289-300.

Cook, F.A., van der Velden, A.J., Hall, K.W., and Roberts, B.J.
1999: Frozen subduction in Canada's Northwest Territories; LITHOPROBE deep lithospheric reflection profiling of the western Canadian Shield; Tectonics, v. 18, p. 1-24.

Cousens, B.L.
2000: Geochemistry of the Archean Kam Group, Yellowknife greenstone belt, Slave Province, Canada; Journal of Geology, v. 108, p. 181-197.

Cousens, B., Facey, K., and Falck, H.
2002: Geochemistry of the late Archean Banting Group, Yellowknife greenstone belt, Slave Province, Canada; simultaneous melting of the upper mantle and juvenile mafic crust; Canadian Journal of Earth Science, v. 39, p. 1635-1656.

Cousens, B., Falck, H., Ootes, L., Jackson, V., Mueller, W., Corcoran, P., Finnigan, C., van Hees, E., Facey, C., and Alcazar, A.
2006: Regional correlations, tectonic settings, and stratigraphic solutions in the Yellowknife greenstone belt and adjacent areas from geochemical and Sm-Nd isotopic analyses of volcanic and plutonic rocks; Chapter 7 *in* Gold in the Yellowknife Greenstone Belt, Northwest Territories: Results of the EXTECH III Multidisciplinary Research Project, (ed.) C.D. Anglin, H. Falck, D.F. Wright, and E.J. Ambrose; Geological Association of Canada, Mineral Deposits Division, Special Publication No. 3, p. 70-94.

Davis, W.J. and Hegner, E.
1992: Neodymium isotopic evidence for the tectonic assembly of Late Archean crust in the Slave Province, northwest Canada; Contributions to Mineralogy and Petrology, v. 111, p. 493-504.

Edwards, R.N., Bailey, R.C., and Garland, G.D.
1981: Conductivity anomalies: lower crust or asthenosphere?; Physics of the Earth and Planetary Interiors, v. 25, p. 263-272.

Falck, H., Cousens, B., and Isachsen, C.
1999: Yet another look at the Yellowknife stratigraphy: Give me a break; 27th Yellowknife Geoscience Forum, INAC Geology Division, Yellowknife, Abstracts, p. 16-18.

Falck, H., Donaldson, J.A., and Hall, L.
1991: Regolith beneath the Archean Jackson Lake Formation; Its implications for Yellowknife volcanic belt stratigraphy, Slave Province, NWT; *in* Geological Association of Canada, Mineralogical Association of Canada Joint Annual Meeting with the Society of Economic Geologists; Abstracts, v. 16, p. 35.

Fernández Viejo, G. and Clowes, R.M.
2003: Lithospheric structure beneath the Archean Slave Province and the Proterozoic Wopmay orogen, northwestern Canada, from a LITHOPROBE refraction/wide-angle reflection survey; Geophysical Journal International, v. 153, p. 1-19.

Fischer, G. and Le Quang, B.V.
1981: Topography and minimization of the stand deviation in one-dimensional magnetotelluric modelling; Geophysical Journal of the Royal Astronomical Society, v. 67, p. 279-292.

Fischer, G., Schnegg, P.A., Peguiron, M., and Le Quang, B.V.
1981: An analytic one-dimensional magnetotelluric inversion scheme; Geophysical Journal of the Royal Astronomical Society, v. 67, p. 257-278.

Gamble, T.D., Goubau, W.M., and Clarke, J.
1979: Magnetotellurics with a remote reference; Geophysics, v. 44, p. 53-68. Reprinted in Vozoff (1986), p. 189-204.

Gough, D.I.
1986: Seismic reflectors, conductivity, water and stress in the continental crust; Nature, v. 323, p. 143-144.

Groom, R.W. and Bailey, R.C.
1989: Decomposition of magnetotelluric impedance tensors in the presence of local three-dimensional galvanic distortion; Journal of Geophysical Research, v. 94, p. 1913-1925.
1991: Analytical investigations of the effects of near surface three-dimensional galvanic scaterers on MT tensor decomposition; Geophysics, v. 56, p. 496-518.

Groom, R.W., Kurtz, R.D., Jones, A.G., and Boerner, D.E.
1993: A quantitative methodology for determining the dimensionality of conductive structure from magnetotelluric data; Geophysical Journal International, v. 115, p. 1095-1118.

Helmstaedt, H.H.
2006: Evolution of the geological understanding of the Yellowknife Domain; Chapter 3 *in* Gold in the Yellowknife Greenstone Belt, Northwest Territories: Results of the EXTECH III Multidisciplinary Research Project, (ed.) C.D. Anglin, H. Falck, D.F. Wright, and E.J. Ambrose; Geological Association of Canada, Mineral Deposits Division, Special Publication No. 3, p. 29-37.

Helmstaedt, H.H. and Padgham, W.A.
1986: A new look at the stratigraphy of the Yellowknife Supergroup at Yellowknife, N.W.T.; Implications for the age of gold-bearing shear zones and Archean basin evolution; Canadian Journal of Earth Science, v. 23, p. 454-475.

Henderson, J.B.
1998: Preliminary Geology, Wijinnedi Lake Area, District of Mackenzie, Northwest Territories; Geological Survey of Canada, Open File 3609, 1 colour map, scale 1:50000.

Henderson, J.F. and Brown, I.C.
1966: Geology and Structure of the Yellowknife Greenstone Belt, District of Mackenzie; Geological Survey of Canada, Bulletin 141, 87 p.

Hyndman, R.D. and Shearer, P.M.
1989: Water in the lower continental crust: Modelling magnetotelluric and seismic reflection results; Geophysical Journal International, v. 98, p. 343-365.

Jones, A.G.
1981: On a type classification of lower crustal layers under Precambrian regions; Journal of Geophysics, v. 49, p. 226-233.
1982: On the electrical crust-mantle structure in Fennoscandia: No Moho and the asthenosphere revealed?; Geophysical Journal of the Royal Astronomical Society, v. 68, p. 371-388.
1986: Parkinson's pointers' potential perfidy!; Geophysical Journal of the Royal Astronomical Society, v. 87, p. 1215-1224.
1988: Static shift of magnetotelluric data and its removal in a sedimentary basin environment; Geophysics, v. 53, p. 967-978.
1992: Electrical conductivity of the continental lower crust; Chapter 3 *in* Continental Lower Crust, (ed.) D.M. Fountain, R.J. Arculus, and R.W. Kay; Elsevier, Amsterdam, p. 81-143.
1993: Electromagnetic images of modern and ancient subduction zones; *in* Plate Tectonic Signatures in the Continental Lithosphere, (ed.) A.G. Green, A. Kroner, H.-J Gotze and N. Pavlenkova; Tectonophysics, v. 286, p. 273-298.
1998: Waves of the future: Superior inferences from collocated seismic and electromagnetic experiments; Tectonophysics, v. 286, p. 273-298.
1999: Imaging the continental upper mantle using electromagnetic methods; Lithos, v. 48, p. 57-80.

Jones, A.G. and Dumas, I.
1993: Electromagnetic images of a volcanic zone; Physics of the Earth and Planetary Interiors, v. 81, p. 289-314.

Jones, A.G. and Ferguson, I.J.
2001: The electric Moho; Nature, v. 409, p. 331-333.

Jones, A.G. and Groom, R.W.
1993: Strike angle determination from the magnetotelluric tensor in the presence of noise and local distortion: rotate at your peril!; Geophysical Journal International, v. 113, p. 524-534.

Jones, A.G. and Jödicke, H.
1984: Magnetotelluric transfer function estimation improvement by a coherence-based rejection technique; 54th Society of Exploration Geophysics Annual General Meeting, Altlanta, Georgia, U.S.A., December 2-6, Abstracts, p. 51-55.

Jones, A.G. and Spratt, J.
2002: A simple method for deriving the uniform field MT responses in auroral zones; Earth, Planets and Space, v. 54, p. 443-450.

Jones, A.G., Chave, A.D., Egbert, G., Auld, D., and Bahr, K.
1989: A comparison of techniques for magnetotelluric response function estimation; Journal of Geophysical Research, v. 94, p. 14,201-14,213.

Jones, A.G., Kurtz, R.D., Boerner, D.E., Craven, J.A., McNeice, G., Gough, D.I., DeLaurier, J.M., and Ellis, R.G.
1992: Electromagnetic constraints on strike-slip fault geometry – the Fraser River fault system; Geology, v. 20, p. 561-564.

Jones, A.G., Snyder, D., Hanmer, S., Asudeh, I., White, D., Eaton, D., and Clarke, G.
2002: Magnetotelluric and teleseismic study across the Snowbird Tectonic Zone, Canadian Shield: A Neoarchean mantle suture?; Geophysical Research Letters, v. 29 p. 10-1–10-4.

Jones, A.G., Lezaeta, P., Ferguson, I.J., Chave, A.D., Evans, R., Garcia, X., and Spratt, J.
2003: The electrical structure of the Slave craton; Lithos, v. 71, p. 505-527.

Katsube, T.J., Kerswill, J., Connell, S., Keating, P., Falck, H., and Scromeda-Perez, N.
2006: Geophysical and petrophysical characteristics of host rocks, alteration zones, and structures associated with gold mineralization in the Yellowknife Domain; Chapter 21 *in* Gold in the Yellowknife Greenstone Belt, Northwest Territories: Results of the EXTECH III Multidisciplinary

Research Project, (ed.) C.D. Anglin, H. Falck, D.F. Wright, and E.J. Ambrose; Geological Association of Canada, Mineral Deposits Division, Special Publication No. 3, p. 325-339.

Kirkwood, S.C., Hutton, V.R.S., and Sik, J.
1981: A geomagnetic study of the Great Glen fault; Geophysical Journal of the Royal Astronomical Society, v. 66, p. 481-490.

Kusky, T.M.
1989: Accretion of the Archean Slave province; Geology, v. 17, p. 63-67.

Larsen, J.C.
1977: Removal of local surface conductivity effects from low frequency mantle response curves; Acta Geodaetica Geophysica et Montanistica Academy Science Hungary, v. 12, p. 183-186.
1989: Transfer functions: Smooth robust estimates by least-squares and remote reference methods; Geophysical Journal International, v. 99, p. 645-663.

Larsen, J.C., Mackie, R.L., Manzella, A., Fiordelisi, A., and Rieven, S.
1996: Robust smooth magnetotelluric transfer functions; Geophysical Journal International, v. 124, p. 801-819.

Laštovicková, M.
1991: A review of laboratory measurements of the electrical conductivity of rocks and minerals; Physics of the Earth and Planetary Interiors, v. 66, p. 1-11.

Ledo, J., Jones, A.G., and Ferguson, I.J.
2002: Electromagnetic images of a strike-slip fault: The Tintina Fault - northern Canadian Cordillera; Geophysical Research Letters, v. 29, p.8-1–8-4.

Mackie, R.L., Livelybrooks, D.W., Madden, T.R., and Larsen, J.C.
1997: A magnetotelluric investigation of the San Andreas Fault at Carrizo Plain, California; Geophysical Research Letters, v. 24, p. 1847-1850.

MacLachlan, K, Relf, C., Cairns, S., Hardy, F., and Davis, B.
2001: New multidisciplinary geological investigations in the Walmsley Lake area, southeastern Slave Province, Northwest Territories; Geological Survey of Canada, Current Research 2001-C4, p. 24.

Marquis, G., Jones, A.G., and Hyndman, R.D.
1995: Coincident conductive and reflective lower crust across a thermal boundary in southern British Columbia, Canada; Geophysical Journal International, v. 120, p. 111-131.

Martel, E. and Lin, S.
2006: Structural evolution of the Yellowknife greenstone belt, with emphasis on the Yellowknife River Fault Zone and the Jackson Lake Formation; Chapter 8 *in* Gold in the Yellowknife Greenstone Belt, Northwest Territories: Results of the EXTECH III Multidisciplinary Research Project, (ed.) C.D. Anglin, H. Falck, D.F. Wright, and E.J. Ambrose; Geological Association of Canada, Mineral Deposits Division, Special Publication No. 3, p. 95-115.

Martel, E., Lin, S., and Bleeker, W.
2002: Kinematic Observations in the Yellowknife River Fault Zone and Structures in the Jackson Lake Formation, Yellowknife Greenstone Belt, Northwest Territories; Geological Survey of Canada, Current Research 2002-E4, 10 p.

McNeice, G. and Jones, A.G.
2001: Multisite, multifrequency tensor decomposition of magnetotelluric data; Geophysics, v. 66, p. 158-173.

Mueller, W.J.A. and Donaldson, P.
1994: Volcanic and Tectono-Plutonic Influences on Sedimentation in the Archean Kirkland Basin, Abitibi Greenstone Belt, Canada; Precambrian Research, v. 68, p. 201-230.

Olhoeft, G.R.
1981: Electrical properties of granite with implications for the lower crust; Journal of Geophysical Research, v. 86, p. 931-936.

Park, S.K. and Mackie, R.L.
2000: Resistive (dry?) lower crust in an active orogen, Nanga Parbat, northern Pakistan; Tectonophysics, v. 316, p. 359-380.

Park, S.K. and Roberts, J.J.
2003: Conductivity structure of the San Andreas fault, Parkfield, revisited; Geophysical Research Letters, v. 30, p.5-1–5-4, DOI 10.1029/2003GL017689.

Parker, R.L.
1980: The inverse problem of electromagnetic induction: existence and construction of solutions based on incomplete data; Journal of Geophysical Research, v. 85, p. 4421-4425.

Parker, R.L. and Whaler, K.A.
1981: Numerical methods for establishing solutions to the inverse problem of electromagnetic induction; Journal of Geophysical Research, v. 86, p. 9574-9584.

Pettijohn, F.J.
1970: The Canadian Shield; a status report, 1970; *in* Basins and geosynclines of the Canadian Shield, (ed.) A.J. Baer; Geological Survey of Canada, Paper 70-40, p. 239-265.

Poll, H.E., Weaver, J.T., and Jones, A.G.
1987: Calculations of voltage differences for magnetotelluric modelling of a region with near-surface inhomogeneities; Physics of the Earth and Planetary Interiors, v. 53, p. 287-297.

Price, A.T.
1973: The theory of geomagnetic induction; Physics of the Earth and Planetary Interiors, v. 7, p. 227-233.

Richards, M.L., Schmucker, U., and Steveling, E.
1982: Entzerrung der Impedanzkurven von magnetotellurischen Messungen in der Schwäbischen Alb; *in* Protokol über das 9 Kolloquium Elektromagnetische Tiefenforschung (Abstracts from 9th Electromagnetic Deep Sounding Symposium), Neustadt, Weinstraße, March 22-26, p. 27-40.

Rodi, W. and Mackie, R.L.
2001: Nonlinear conjugate gradients algorithm for 2-D magnetotelluric inversion; Geophysics, v. 66, p. 174-187.

Schmucker, U.
1970: Anomalies of Geomagnetic Variations in the Southwestern United States; Bulletin of the Scripps Institute of Oceanography, University of California Press, v. 13, 165 p.

Scromeda, N., Connell, S., Katsube, T.J., and Mwenifumbo, J.
2000: Petrophysical Properties of Mineralized and Non-Mineralized Rocks from Giant and Con Mine Areas, Northwest Territories; Geological Survey of Canada, Current Research 2000-E8, 7 p.

Smith, J.T.
1995: Understanding telluric distortion matrices; Geophysical Journal International, v. 122, p. 219-226.
1997: Estimating galvanic-distortion magnetic fields in magnetotellurics; Geophysical Journal International, v. 130, p. 65-72.

Snyder, D.B., Bleeker, W., Roberts, B.J., and Salisbury, M.D.
2006: Structure and crustal architecture of the Yellowknife greenstone belt from SNORCLE geophysical survey data; Chapter 9 *in* Gold in the Yellowknife Greenstone Belt, Northwest Territories: Results of the EXTECH III Multidisciplinary Research Project, (ed.) C.D. Anglin, H. Falck, D.F. Wright and E.J. Ambrose; Geological Association of Canada, Mineral Deposits Division, Special Publication No. 3, p. 116-125.

Stern, R.A. and Bleeker, W.
1998: Age of the world's oldest rocks refined using Canada's SHRIMP: The Acasta Gneiss Complex, Northwest Territories, Canada; Geoscience Canada, v. 25, p. 27-31.

Stubley, M., Siddle, J., and Bleeker, W.
1997: The Ormsby break; crustal-scale control on gold mineralization on the Discovery property, southern Slave Province; *in* NWT Geoscience Forum 25th Anniversary, Yellowknife; Program and Abstracts of Talks and Posters, p. 92-93.

Tikhonov, A.N.
1950: On determining electric characteristics of the deep layers of the Earth's crust. Doklady Akademii Nauk, SSSR, v. 73, p. 295-297. Reprinted in Vozoff (1986), p. 2-3.

Thorpe, R.I., Cumming, G.L., and Mortensen, J.K.
1992: A significant Pb isotope boundary in the Slave Province and its probable relation to ancient basement in the western Slave Province; *in* Project Summaries, Canada-Northwest Territories mineral development subsidiary agreement; Geological Survey of Canada, Open File Report 2484, p. 279-284.

Unsworth, M.J., Malin, P.E., Egbert, G.D., and Booker, J.R.
1997: Internal structure of the San Andreas Fault at Parkfield, California; Geology, v. 25, p. 359-362.

Unsworth, M., Egbert, G., and Booker, J.R.
1999: High-resolution electromagnetic imaging of the San Andreas Fault in central California; Journal of Geophysical Research, B, Solid Earth and Planets, v. 104, p. 1131-1150.

van der Velden, A. and Cook, F.A.
2002: Products of 2.65-2.58 Ga orogenesis in the Slave Province correlated with Slave-Northern Cordillera lithospheric evolution (SNORCLE) seismic reflection patterns; Canadian Journal of Earth Science, v. 39, p. 1189-1200.

Vozoff, K. (editor)
1986: Magnetotelluric Methods; Society of Exploration Geophysics, Geophysics Reprint Series No. 5, Tulsa, OK, 736 p.

Wannamaker, P.E.
1997: Comment on "The petrologic case for a dry lower crust", by Yardley, B.W.D., and J.W. Valley; Journal of Geophysical Research, v. 102, p. 12,173-12,185.

Weidelt, P.
1972: The inverse problem of geomagnetic induction; Zetischrift für Geophysik, v. 38, p. 257-289.

Wiggins, R.A.
1972: The general linear inverse problem: Implications of surface waves and free oscillations for Earth structure; Reviews of Geophysics and Space Physics, v. 10, p. 251-285.

Wight, D.E. and Bostick, F.X.
1980: Cascade decimation - a technique for real time estimation of power spectra; Proceedings of the IEEE International Conference on Acoustics, Speech, and Signal Processing, p. 626-629. Denver, CO, April 9-11. Reprinted in Vozoff (1986).

Wu, X., Ferguson, I.J., and Jones, A.G.
2002: Magnetotelluric response and geoelectric structure of the Great Slave Lake shear zone; Earth and Planetary Science Letters, v. 196, p. 35-50.

Yardley, B.W.D. and Valley, J.W.
1997: The petrologic case for a dry lower crust; Journal of Geophysical Research, v. 102, p. 12,172-12,185.

Zhang, P., Roberts, R.G., and Pedersen, L.B.
1987: Magnetotelluric strike rules; Geophysics, v. 52, p. 267-278.

Figure 9-C5. Details of SNORCLE line 1 east of Yellowknife and the Yellowknife River (Fig. 9-1). Red boxes indicate the same areas in the subfigures. **a)** Reprocessed reflection section using limited offset range to enhance near-surface reflections. Prominent deep reflections can be traced to within 100 ms (300 m) of the surface. The purple bar represents the Duck Lake Intrusive Sheet gabbro; the blue-green lines show the orientation of foliation planes mapped within the Burwash metaturbidites (Henderson, 1985) as projected onto this section. **b)** P-wave velocity model from tomographic inversion of first breaks on shot gathers. Red are higher velocities (>6.2 km s^{-1}); some coincide with the mapped location of the Duck Lake Intrusive Sheet. **c)** Interval velocities used to reprocess the section shown in (a); again higher velocities correlate with the Duck Lake Intrusive Sheet, its depth projection (reflector Y1) and a deeper reflection (Y2 of Cook et al., 1999).

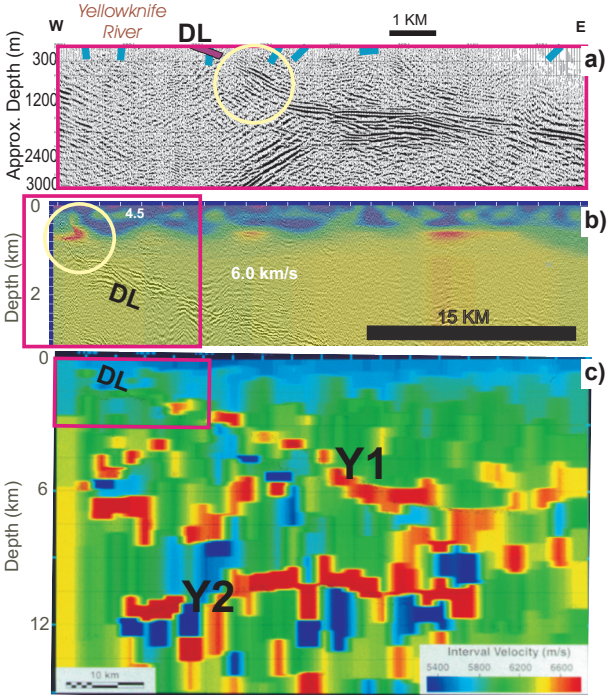

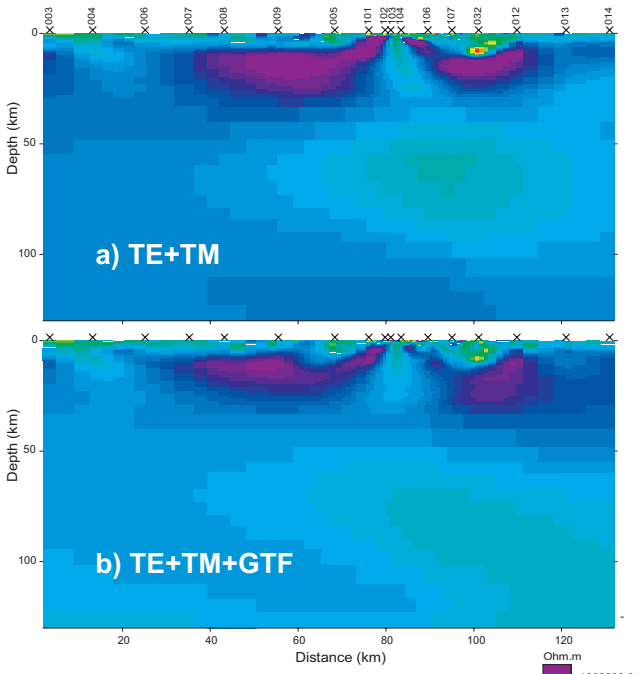

Figure 10-C9. Two-dimensional models of the data from seventeen sites along the profile. **(a)** Model of the TM+TM data. **(b)** Model of the TE+TM+GTF data.

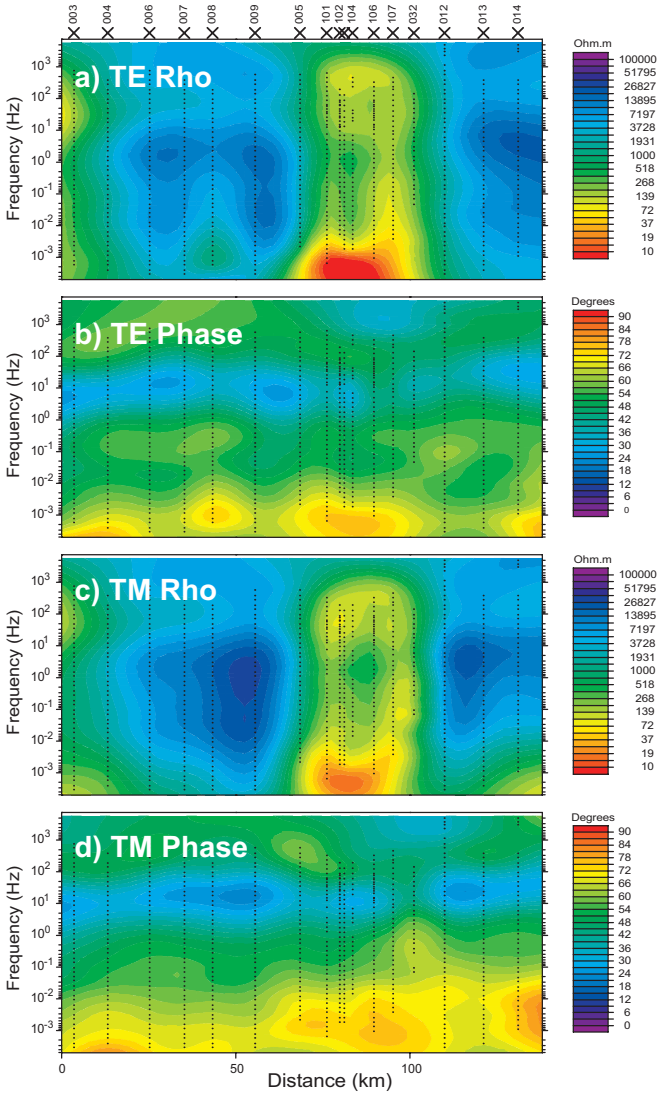

Figure 10-C5. Pseudosections of the apparent resistivity and phase data in the two modes, TE and TM.

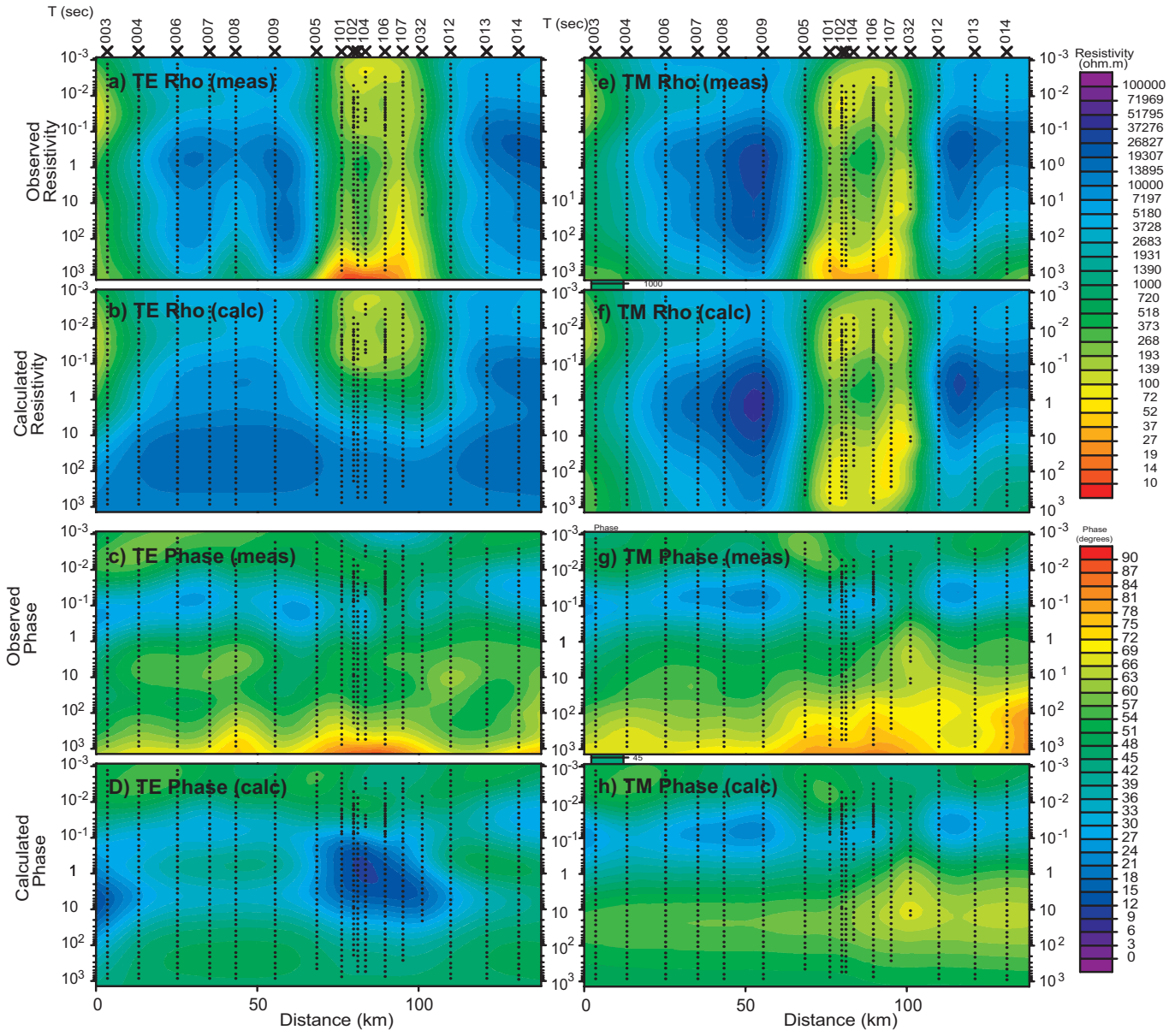

Figure 10-C10. Comparison of the data to the model responses for the TE+TM model (Fig. 10-8a).

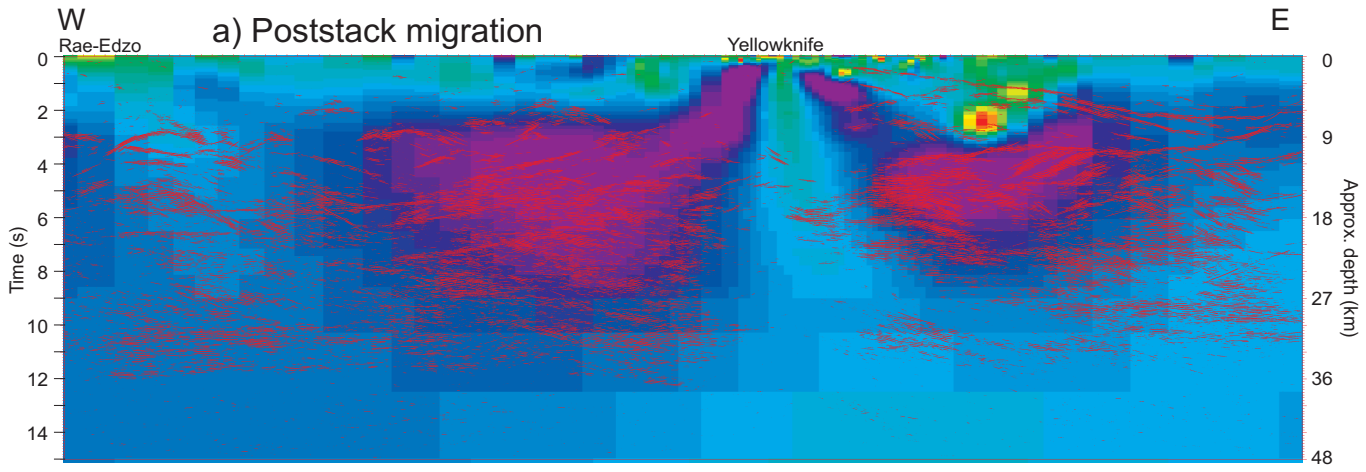

Figure 10-C11. Seismic reflection migrated data and interpretation from Profile 1 of van der Velden and Cook (2002). The MT model has been distorted on either side of Yellowknife in order to take account of the road direction along which the seismic reflection data were acquired. **(a)** Migrated seismic reflection data on top of the resistivity model.

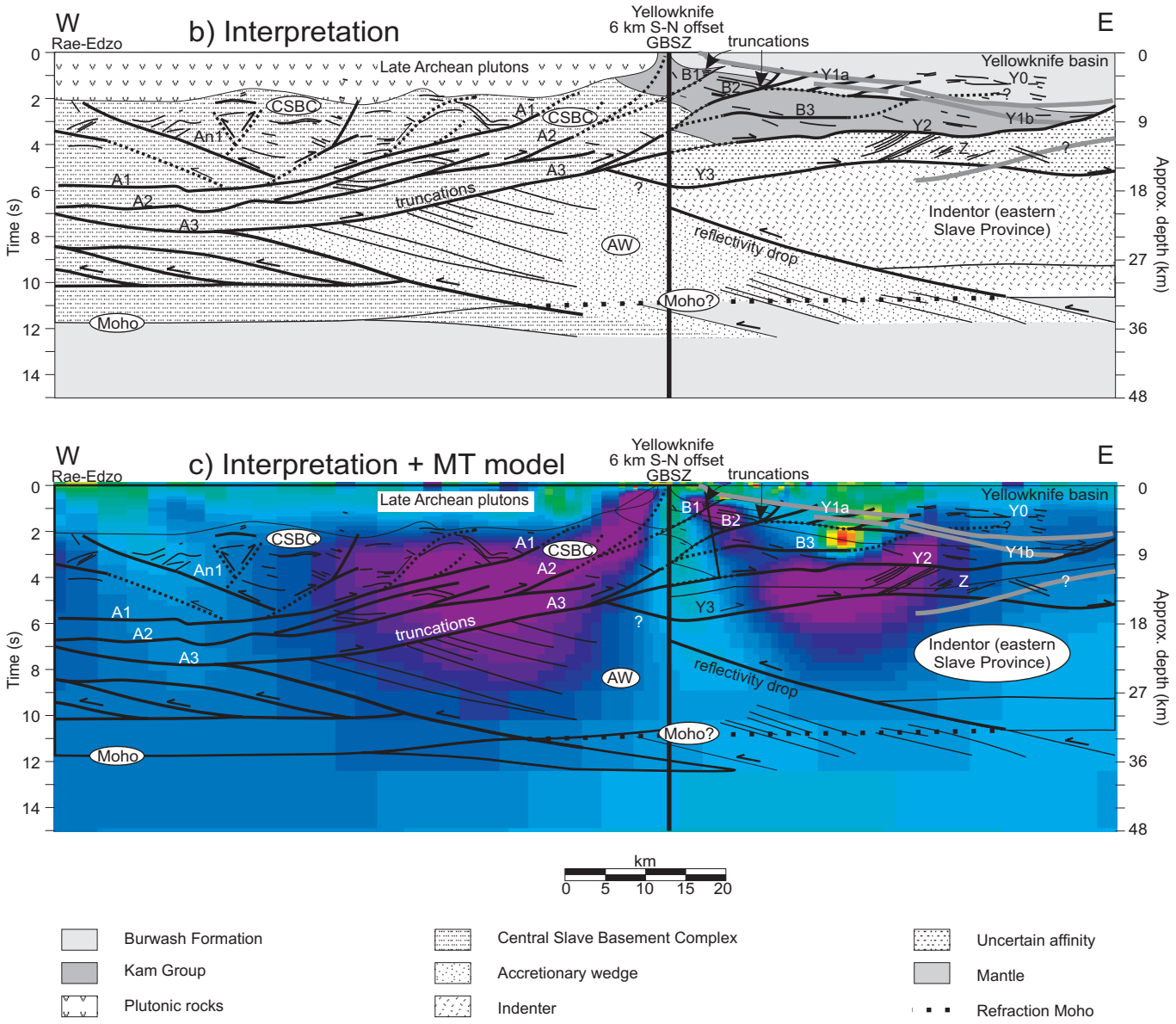

Figure 10-C11 continued. **(b)** Interpretation by van der Velden and Cook (2002). **(c)** Comparison of the van der Velden and Cook (2002) interpretation with the resistivity model. (CSBC = Central Slave Basement Complex, GBSZ = gold-bearing shear zones)

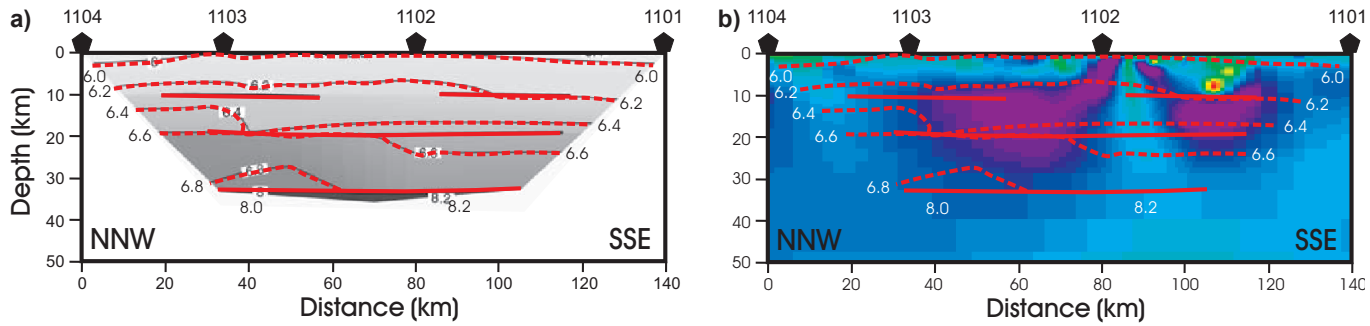

Figure 10-C12. Principle results from the seismic refraction experiment along the profile. **(a)** Seismic refraction model (redrawn from Fernández Viejo and Clowes, 2003). **(b)** Main interfaces from the refraction model compared to the TE+TM resistivity model (Fig. 10-8a).